 doi:10.20944/preprints201907.0340.v1

Article

Wire Ropes and CFRP Strips to Provide the Masonry Walls with Out-of-Plane Strengthening

Elena Ferretti

Department of Civil, Environmental and Materials Engineering – DICAM, Alma Mater Studiorum Università di Bologna, 40136 Bologna, Italy; elena.ferretti2@unibo.it; Tel.: +39-051-209-35-15

Abstract: The present paper deals with an improvement of the strengthening technique consisting in the combined use of straps—made of stainless steel ribbons—and CFRP strips, to increase the out-of-plane strength of masonry walls. The straps of both the previous and the new combined technique pass from one face to the opposite face of the masonry wall through some holes made along the thickness, giving rise to a three-dimensional net of loop-shaped straps, closed on themselves. The new technique replaces the stainless steel ribbons with steel wire ropes, which form closed loops around the masonry units and the CFRP strips as in the previous technique. A turnbuckle for each steel wire rope allows the closure of the loops and provides the desired pre-tension to the straps. The mechanical coupling—given by the frictional forces—between the straps and the CFRP strips placed on the two faces of the masonry wall gives rise to an I-beam behavior of the facing CFRP strips, which begin to resist the load as if they were the two flanges of the same I-beam. Even the previous combined technique exploits the ideal I-beam mechanism, but the greater stiffness of the steel wire ropes compared to the stiffness of the steel ribbons makes the constraint between the facing CFRP strips stiffer. This gives the reinforced structural element greater stiffness and delamination load. In particular, the experimental results show that the maximum load achievable with the second combined technique is much greater than the maximum load provided by the CFRP strips. Even the ultimate displacement turns out to be increased, allowing us to state that the second combined technique improves both strength and ductility. Since the CFRP strips of the combined technique run along the vertical direction of the wall, the ideal I-beam mechanism is particularly useful to counteract the hammering actions provided by the floors on the perimeter walls, during an earthquake. Lastly, after the building went out of service, the box-type behavior offered by the three-dimensional net of straps prevents the building from collapsing, acting as a device for safeguarding life.

Keywords: masonry buildings; hammering actions; out-of-plane strengthening; three-dimensional strengthening systems; CFRP strips; textile reinforced mortar (TRM)

1. Introduction

This paper is part of a research project on improving the out-of-plane behavior of masonry walls by combining different strengthening techniques [1–4]. The key-idea of the combined technique is to exploit friction in order to achieve a mechanical coupling between different strengthening devices. Due to the mechanical coupling, the strengthening devices work together giving rise to a new resistant mechanism, with strengthening characteristics different from those of each constituent strengthening device. Consequently, the resistant mechanism of the combined technique is not simply a combination of the main features of the constituent techniques.

Specifically speaking, the combined technique proposed in [1] and [4] makes use of FRP (Fiber Reinforced Polymer) strips tied by stainless steel straps. The friction at the interface between FRP strips and masonry walls adds a physical bond to the chemical bond provided by the resin alone. As shown in Figure 1, this modifies the limit surface of the interface bond—which becomes a cohesive physical bond—allowing the FRP strips to withstand higher shear forces before delaminating from

Preprints (www.preprints.org) | NOT PEER-REVIEWED | Posted: 30 July 2019 doi:10.20944/preprints201907.0340.v1

the masonry wall under bending loads. This ultimately means that the stretched FRP strip will undergo delamination for higher values of the bending load.

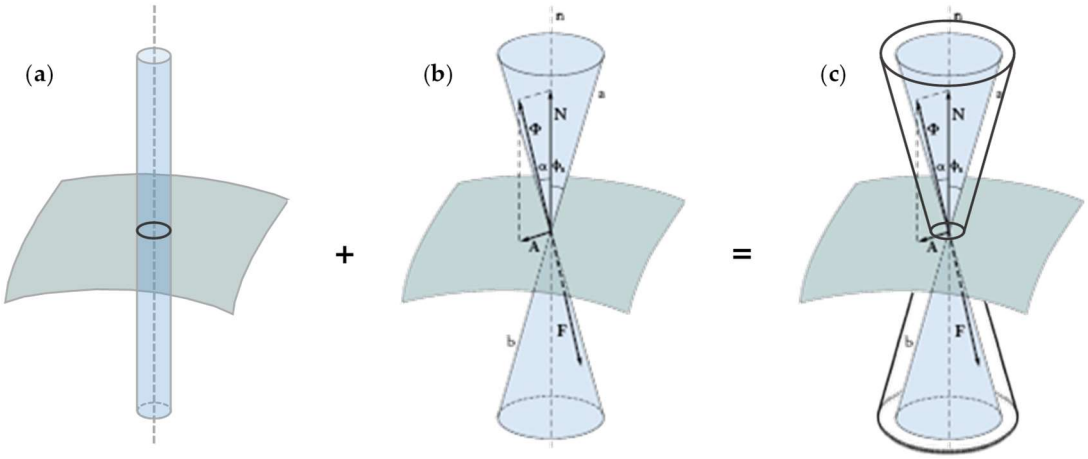

Figure 1. Limit surfaces in static conditions: (**a**) limit surface of the chemical bond, with the shear forces that determine the limit condition, independently of the compression forces, (**b**) cone of static friction, and (**c**) cone of cohesive static friction, which results from the combination between the limit surface of the chemical bond and the cone of static friction [1].

As far as the meaning of symbols in Figure 1 is concerned:

- **N** is the normal force, developed by the support plane as a reaction to the force, **P**, exerted by the body on the support plane (body 1 in Figure 2): **N** is equal and opposite to **P**;
- **A** is the frictional force, developed by the support plane as a reaction to the shear force **T** (exerted by body 2, the hanging body in Figure 2): in static conditions, **A** is equal and opposite to **T**;
- **F** is the resultant force acting on the support plane (the component vectors of **F** are **P** and **T**);
- **Φ** is the resultant force acting on the body on the support plane (the component vectors of **Φ** are **N** and **A**);
- $\alpha = \tan^{-1} A/N$ is the angle formed by **Φ** with the direction orthogonal to the support plane;
- ϕ_s is the angle of static friction, that is, the maximum inclination angle of the support plane before which the body will begin sliding on it;
- $\tan \phi_s$ is the coefficient of static friction, which is a dimensionless scalar value that describes the maximum ratio of the force of friction between two bodies at rest relative to each other and the force pressing them together.

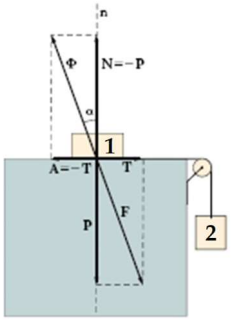

Figure 2. Forces at the interface between a body at rest (body 1) and its support plane.

Since the frictional force **A** develops as reaction force to counteract the relative sliding at the interface between two bodies when a normal force **P** presses the two bodies together, to take

 doi:10.20944/preprints201907.0340.v1

advantage of the beneficial effect of friction it is necessary to push the FRP strips against the masonry wall. The device used at an early stage of the research program to push the FRP strips against the masonry wall is the CAM (Active Confinement of Masonry) system [5–12], a continuous three-dimensional net of stainless steel straps that post-compress the wrapped masonry by means of a pre-tension of the straps. Therefore, the CAM system is an active strengthening system that belongs to the strengthening category of "horizontal and vertical ties", one of the four categories of strengthening techniques considered in the Italian seismic codes [13,14]. This category is particularly useful in cases of lack of transversal links and ineffective connections between walls or between walls and floors, as usual in historical buildings [6,7,15–29].

The main target of the CAM system, patented in 1999 by Dolce and Marnetto, is to provide the wrapped masonry with an additional state of hydrostatic stress, which increases the safety factor of the masonry building. Nevertheless, a more accurate analysis of the actual stress-transfer mechanism from the CAM net to the masonry wall [2,3] showed that the additional state of stress provided by the CAM system is not hydrostatic. In the specific case of a rectangular CAM net, for instance, the nodes of the CAM net receive pairs of equal and opposite forces in the plane of the wall and not balanced forces in the thickness of the wall (Figure 3). Consequently, the retrofitting system does not transfer any in-plane force to the nodes of the rectangular CAM net, while it compresses the masonry wall along the transverse direction.

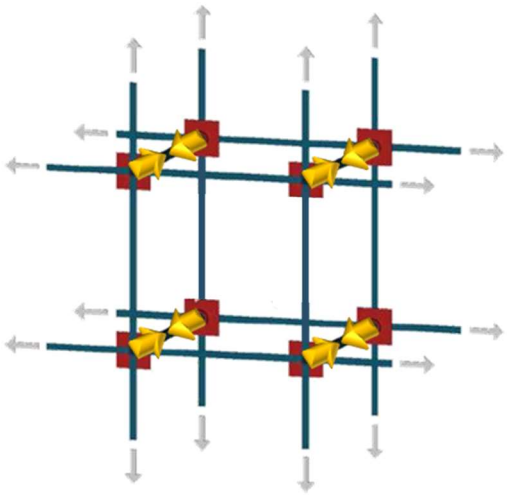

Figure 3. Scheme of stress transfer from the CAM system to the masonry wall: balanced forces in gray and not balanced forces in yellow [1].

By providing compression forces only along the thickness of the wall, the straps of the CAM system, deprived of their original use, find a new employment in the combined technique as devices to push the FRP strips against the masonry wall. In fact, if applied over the FRP strips, the pre-tension of the straps pushes the FRP strips against the masonry wall in the same way as the vertical force of Figure 2 compresses body 1 against its support plane. On the stretched side of a bent beam, this modifies the interface bond of the FRP strips from a chemical to a cohesive physical bond (Figure 1), increasing the delamination load by means of the frictional effect. In other words, the compression forces exerted by the straps on the FRP strip modify the shape of the limit surface, from the cylinder of Figure 1a to the double truncated cone of Figure 1c, allowing the FRP strip to withstand higher shear forces before the head of Φ touches the limit surface. Therefore, the strapping delays the delamination on the stretched side.

A useful application of the straps/strips combined technique consists in placing the FRP strips vertically, one in front of the other on the two opposite faces of a masonry wall (Figure 4). In this case, an additional advantage in terms of reinforcement overlaps with the benefits of the cohesive physical bond on the stretched side: when tied together by the CAM straps as in Figure 4, two facing FRP strips behave like the two flanges of an ideal FRP I-beam (Figure 5). As soon as the FRP strips begin to work together due to the transverse connection established by the CAM system, the strengthening

Preprints (www.preprints.org) | NOT PEER-REVIEWED | Posted: 30 July 2019 doi:10.20944/preprints201907.0340.v1

effect under bending loads becomes the same as that provided by an embedded buttress, with the great advantage of not having to cut the masonry wall to insert an I-beam.

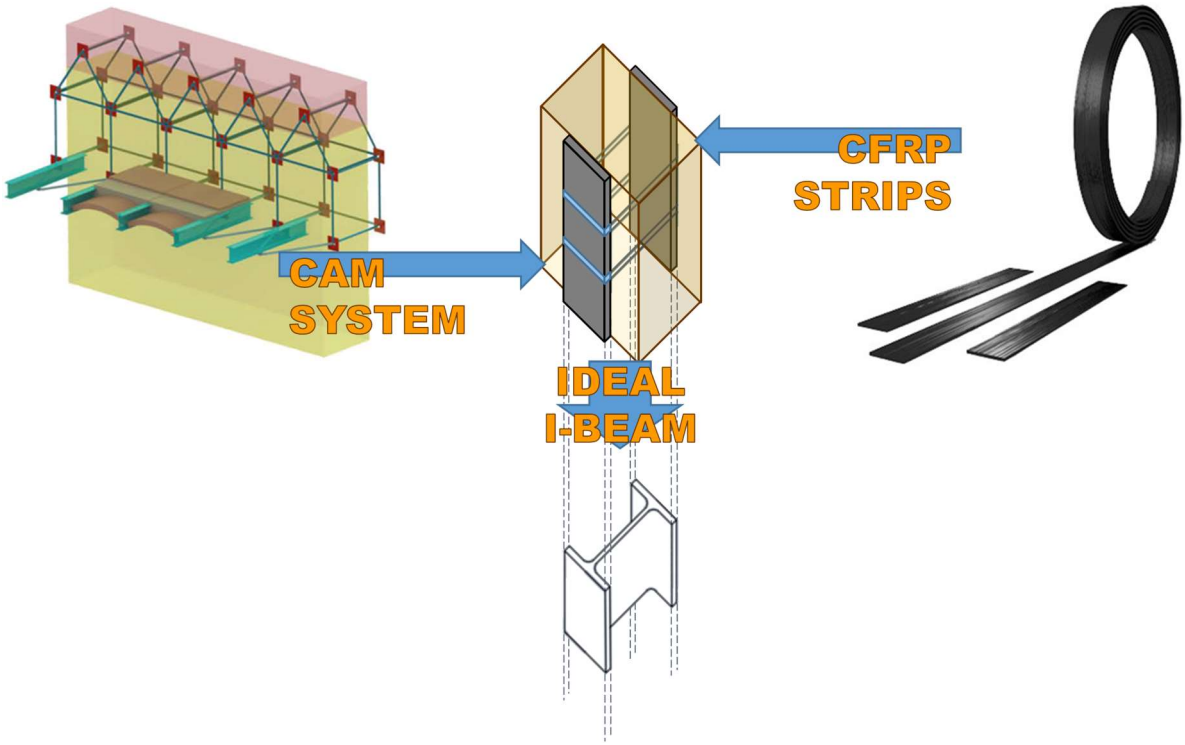

Figure 4. The mechanical coupling between the ribbons of the CAM system and the FRP strips provides a bracing effect in the thickness, which is similar to that given by an embedded I-beam [1].

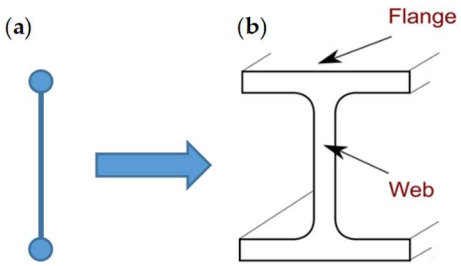

Figure 5. Concept of the straps/strips combined technique: two FRP strips tied by CAM ribbons behave as (**a**) two mass points connected by a stiffness constraint, which is the ideal scheme of behavior of (**b**) a bent I-beam in its cross-section.

Since the mechanical coupling between the two facing FRP strips increases the moment of inertia of the strengthening device considerably [4], the incremental strength given by the ideal I-beam is much greater than that given by the FRP strips taken singularly. Moreover, the strengthening effect of the embedded buttress is the more remarkable the thicker the masonry wall, because a greater wall thickness increases the moment of inertia of the ideal I-beam [4]. Actually, the masonry wall enclosed between the two FRP strips acts as a lost formwork, as it serves to fix the distance between the two flanges of the ideal I-beam, that is, the web high of the ideal I-beam (Figure 5).

Furthermore, since the CAM net crosses the floors easily [1], the ideal I-beam can extend to the entire height of a building. Consequently, the ideal I-beam is able to counteract the horizontal displacements caused by the hammering actions of the floors on the perimeter walls, during a seismic event, when the earthquake direction is orthogonal to the walls of a multi-story building. This latter feature is of paramount importance to counteract the catastrophic collapses of URM buildings, which imply serious loss of life. In fact, observations from earthquakes in the past have shown that the catastrophic collapses of the URM walls are more likely to occur exactly in the out-of-plane direction.

Preprints (www.preprints.org) | NOT PEER-REVIEWED | Posted: 30 July 2019 doi:10.20944/preprints201907.0340.v1

The use of buttresses is just one of the most ancient techniques developed over the centuries for the retrofit/strengthening of URM (Unreinforced Masonry) structures. In its original use, where buttresses were structures built against or projecting from a wall, this ancient technique is effective but highly invasive and causes great increases in mass. As a result, with the advent of new technologies, buttresses were gradually abandoned in favor of more recent strengthening techniques, some of which are base isolation, seismic dampers, surface treatments, mortar joint treatments, external steel reinforcement, post-tensioning, mesh reinforcement, reticulatus system, confinement with ring beams, tie bars, and fiber/textile-reinforced mortar [2, 30–32]. The straps/strips combined technique recuperates the simple strengthening scheme of the buttress, but minimizing invasiveness and mass increases. The ability of the combined technique to provide an out-of-plane cross-bracing of walls in masonry buildings is all the more remarkable precisely because it allows us to obtain the same strengthening mechanism as an embedded buttress without a significant increase in the mass of the building. In fact, a significant increase in mass is particularly harmful for the building, because it increases the attraction of seismic forces.

Lastly, by obtaining the same effect as a buttress with the use of the CAM system it is possible to enrich the out-of-plane cross-bracing device with characteristics not owned by either traditional buttresses, or the most recent strengthening techniques. In fact, the three-dimensional continuous net of the CAM system establishes good connections between all the structural elements of a building and allows the combined technique to guarantee the so-called box-type behavior—one of the main concerns in retrofitting masonry buildings [33–35]—that consists in tying the building elements to each other, starting from the building foundation (Figure 6). As a result, the building moves as a single unit, insuring a coherent load path for lateral loads, reduction of out-of-plane wall failures, reduction of loss of support for floors and roofs, and reduction of falling parapets or ornamentation.

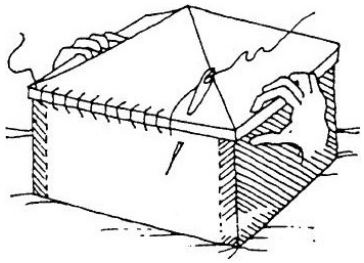

Figure 6. The effectiveness of structural connections provides box-type behavior to the building.

2. The straps/strips combined technique

As detailed in Section 1, the straps/strips combined technique is an out-of-plane strengthening technique that developed as an improvement of the CAM system. Similarly to the CAM system:

- It consists of a three-dimensional continuous retrofitting system that establishes good connections between all the structural elements of a building, leading to an overall box-type behavior of the retrofitted building (Figure 6).
- It establishes good transversal connections, which are particularly useful when the masonry wall is made of two or more weakly connected vertical layers.
- It makes use of stainless steel straps that form closed loops passing through some holes, obtained by drilling the thickness of the masonry wall. The use of stainless steel avoids the occurrence of corrosion [36] and compatibility [37] problems.
- It is an active reinforcement technique, since a special tool provides a pre-tension to the straps when closing the loops. The pre-tensioned straps post-compress the masonry enclosed inside them starting from the moment of their clamping, without requiring that a structural damage occurs to start working.
- It makes use of special protective elements at the loop corners, to avoid damage due to concentration of stresses at the corners.
- It is easily concealable under a plaster layer because the thicknesses of the straps and the protective elements are of the same order of magnitude as the thickness of the

Preprints (www.preprints.org) | NOT PEER-REVIEWED | Posted: 30 July 2019 doi:10.20944/preprints201907.0340.v1

plaster. Therefore, from an aesthetic point of view it is minimally invasive and suitable for strengthening masonry structures of historical interest.

- It can follow any irregular horizontal or vertical morphology of the wall, making it possible to strengthen even ornamented or complex-shaped walls.
- It does not increase the total weight of the structure too much, making it possible to avoid further attraction of seismic forces.
- It continues to wrap the masonry even after masonry crushing, allowing the damaged wall to keep standing. This high degree of ductility after retrofitting (Figure 7) is of paramount importance for safeguarding life, as people do not risk that some part of the structure hits them, due to the building collapse. Therefore, the combined technique acts as a reinforcement system before the structural damage occurs and a protection device after the structural damage had occurred.

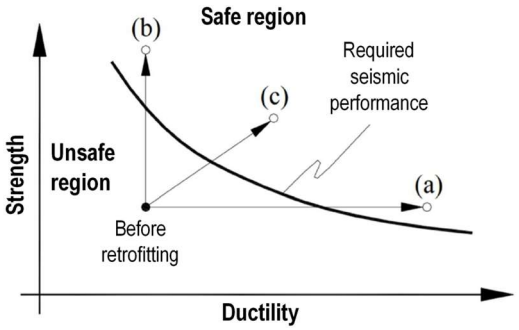

Figure 7. Comparison between the retrofitting systems used to allow an unsafe structure to reach the safe region for seismic loads: an FRP reinforcement increases strength but not ductility, leading the structure to the point (b) along the vertical path; the CAM system and, more in general, a three dimensional reinforcement with steel ribbons increases ductility but not strength, leading the structure to the point (a) along the horizontal path; the combined reinforcement increases both strength and ductility, leading the structure to the point (c).

Moreover, the combined technique inherits from the technology of the composite materials the ability to increase the out-of-plane maximum load of the masonry wall (Figure 7). This is essential to improve the performance of the masonry wall when subjected to hammering actions, for example by the floors.

It is worth noting that, due to the mechanical coupling, the combined technique is not simply the result of using two strengthening techniques together, but something different from both constituent strengthening systems. In particular, the combined technique takes advantage of the beam-like mechanism, which allows the FRP strips to work even after delamination, ensuring a residual load-bearing capacity higher than that provided by the straps alone.

To date, the experimental investigations on the combined technique made use of straps obtained from both steel ribbons—as for the CAM system—and steel wire ropes. Sections 2.1 and 2.2 will deal with both possible techniques, namely, the first combined technique and the second combined technique.

2.1. First Combined Technique: Straps Made of Steel Ribbons

This combined technique is the first attempt to achieve a cross-bracing effect in the thickness of the masonry wall by using steel straps and FRP strips.

The technique inherits from the CAM system the use of stainless steel ribbons to make the straps, but the type of ribbons and the clamping system are not the same as those of the patented CAM system [1]. In particular, as far as the steel ribbons of the first combined technique are concerned, the strength was much lower and the ductility much greater, respectively, than the strength and ductility of the straps used with the patented CAM system [1].

Preprints (www.preprints.org) | NOT PEER-REVIEWED | Posted: 30 July 2019 doi:10.20944/preprints201907.0340.v1

Figure 8 shows a sealed ribbon and the manual device used to provide a pre-tension to the ribbons during strapping.

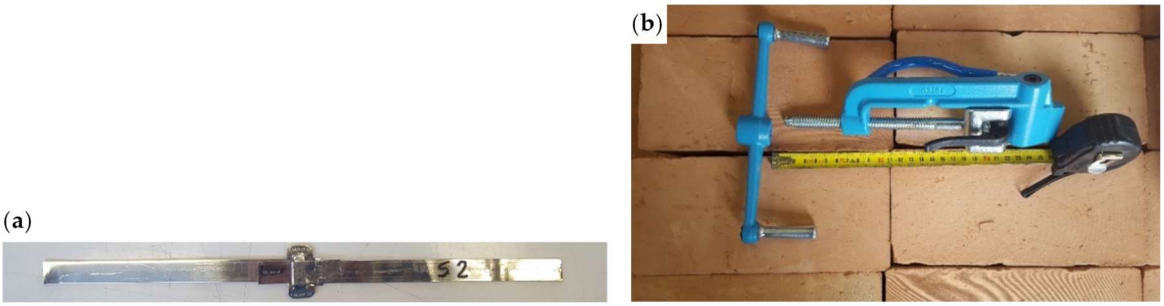

Figure 8. The fastening system of Reference [1]: (**a**) one fastened specimen for the characterization of the junctions and (**b**) the manual strapping tool used to fasten the steel ribbons.

The authors of References [1,4] showed the results of three-point bending flexural tests performed on three wall specimens (Figure 9), strengthened by a three-dimensional net of steel ribbons (Specimen W1), two CFRP (Carbon Fiber Reinforced Polymer) strips (Specimen W2), and a net of steel ribbons and two CFRP strips (Specimen W3). The number of straps per loop for both specimens W1 and W3 was the minimum allowed by the CAM system: just one strap per loop. After testing, the experimenters restored Specimen W3, modified the number of straps per loop as shown in Figure 9, and tested the restored specimen (Specimen W4) by performing a further three-point bending flexural test (for details on the reason for the diversified number of straps per loop of Specimen W4, see [1]).

The purpose of these early flexural tests was to provide some initial indications on how it is actually possible, or not, to obtain an I-beam behavior through the mechanical coupling of steel ribbons and CFRP strips. In the spirit of this first investigation, the tests did not involve any dynamic action. Therefore, the obtained results are not sufficient to draw definitive conclusions on the effectiveness of the combined technique against hammering actions due to seismic actions.

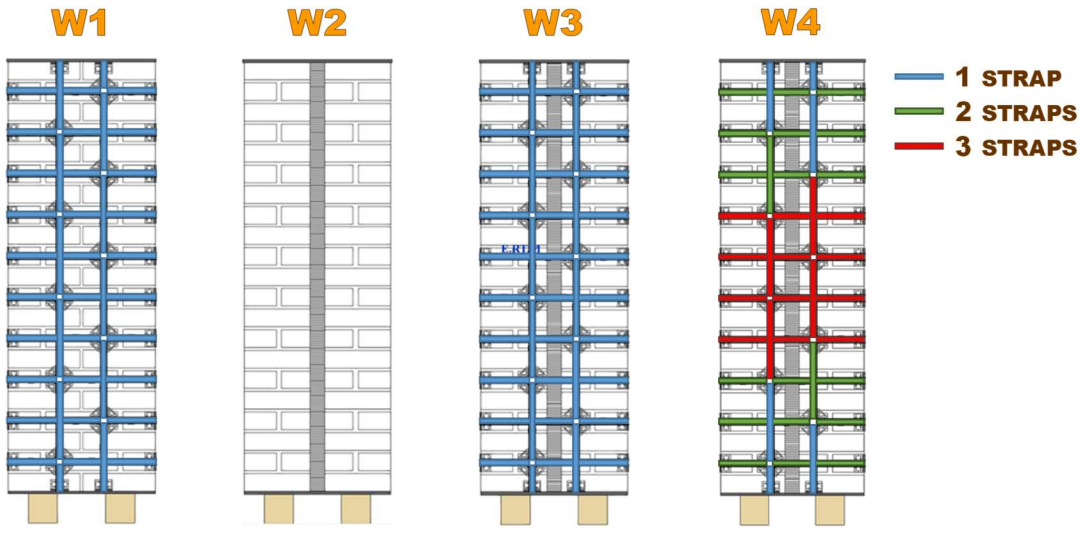

Figure 9. Strengthening schemes of Specimens W1, W2, W3, and W4.

The three-point bending flexural tests on the four specimens took place in the displacement control, after having overturned the specimens of Figure 9 in horizontal configuration.

During the flexural tests, some Linear Variable Differential Transformers (LVDTs) acquired the absolute displacements at the ends and the middle points on the lower faces. The deflections in Figure 10—where the load/deflection diagram of Specimen W3 is much shorter than those of Specimen W1 and Specimen W4 because the instrumentation setup prompted the operator to interrupt the flexural

test well in advance—are the relative displacements in the middle points on the lower faces, calculated as the differences between the absolute displacements acquired.

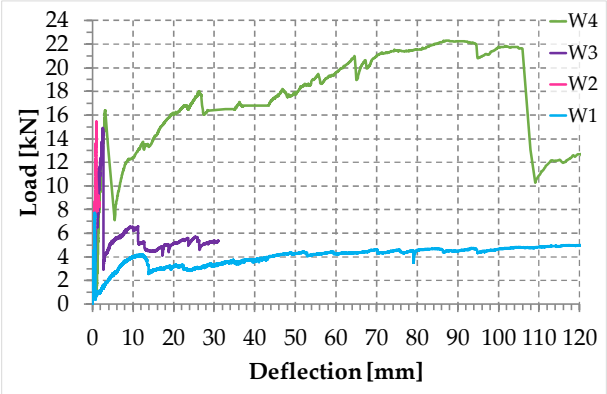

Figure 10. The load/deflections diagrams for the four specimens of the experimentation on the first combined technique.

The load/deflection diagrams in Figure 10 clearly show how the combined technique increases both strength and ductility, allowing the strengthened specimens to reach the point (c) of Figure 7. In particular, the maximum loads for Specimens W3 and W4 are comparable to that given by the CFRP strips alone (about twice the failure load of the masonry wall) and the post-peak behavior is as ductile as that offered by the steel straps alone (Specimens W1). Actually, due to the high ductility, Specimens W1, W3, and W4 did not experienced a real collapse and the operator had to stop the test for such a vertical displacement as to avoid instrumentation damages, while the specimens would have withstood further increases in displacement.

As already pointed out, the high ductility is associated with the ability of the CAM net to retain damaged material, protecting people from possible impact injuries. This is much more important than the ductility itself and is a value added of the combined technique.

The four peaks in Figure 10 return the load values for which the inner hinges open, with disconnection along a mortar bed joint. For Specimens W2, W3 and W4 they also return the loads of delamination.

As far as Specimens W3 and W4 are concerned, the existence of post-delamination paths with loads higher than the post-peak loads of Specimen W1 (retrofitted only with steel straps) indicates that the steel straps retain the delaminated strips, allowing the specimens to benefit from the strengthening effects of both CFRP strips even after delamination.

In other words, the I-beam mechanism survives delamination, although with a decreased stiffness. Actually, the stiffness of the transverse connection after delamination depends on the number of ribbons per loop. In fact, from the comparison between the post-delamination paths of Specimens W3 and W4, it follows that increasing the number of straps per loop also increases the load-bearing capacity after delamination, which means that the ideal I-beam of Specimen W4 is stiffer than the ideal I-beam of Specimen W3.

It is precisely the post-peak behavior described above that allows us to affirm that the combined technique is not simply the result of using two strengthening techniques together, but something different from both constituent strengthening systems. In fact, if the combined technique were a simple sum of the two constituent strengthening techniques, the loads along the post-delamination paths of Specimens W3 and W4 would not be greater than the post-peak loads of Specimen W1. On the contrary, by coupling two techniques created to provide a strengthening effect in the wall plane, the frictional forces caused by the mechanical coupling modify the strengthening mechanism from an in-plane to an out-of-plane mechanism (the ideal I-beam). This allows the combined technique not only to benefit from the main advantages offered by both the CAM system and the CFRP strips, but also to provide a strengthening mechanism that is impossible to achieve with both strengthening techniques, taken individually.

Preprints (www.preprints.org) | NOT PEER-REVIEWED | Posted: 30 July 2019 doi:10.20944/preprints201907.0340.v1

The greater number of longitudinal straps near to the middle cross-section of Specimen W4 (Figure 9) also increases the load-bearing capacity of the specimen at the formation of the inner hinge, which decreases the load drop at delamination (Figure 10). Even the increased number of transverse straps cooperates to increase the residual load after delamination, which further decreases the load drop at delamination. This improves the overall behavior of the strengthened structural element in real applications, since excessive load drop may cause several instability-related issues and load redistribution in the building, which may trigger the collapse of adjacent structural elements.

Actually, the residual load after delamination in Specimen W4 is still too low to avoid instability or damage problems in the adjacent structural elements (of a real building) due to load redistribution, since a load drop of 15% to 20% is the limit usually considered satisfactory to prevent such phenomena from occurring. Nevertheless, having increased the residual load from 20% (Specimen W3) to 43% (Specimen W4) of the delamination load despite the low stiffness of the steel ribbons is a satisfactory result in the spirit of a first investigation, since it certifies the effectiveness of the combined technique in any case.

Furthermore, Specimen W4 is extremely resilient (to such an extent as to be comparable to FRP wrapped columns [38–41]) and allows the regaining of the post-delamination load, which maintains values that are much higher than those of Specimen W3. Even the reason for the load regaining lies in the positive contribution of increasing the number of steel straps and depends on the I-beam behavior of the two CFRP strips.

Since there exists a vertical displacement value for which the post-delamination load is equal to the delamination load and tends to increase further, if the three-point bending flexural test takes place in the load control, the load/deflection diagram of Specimen W4 between the delamination load and the recovered load of post-delamination follows the horizontal path shown in Figure 11. The increase in load after the horizontal path of Figure 11 is of fundamental importance for the overall stability in real applications. In fact, if the retrofitted wall is able to find a new equilibrium configuration at a constant load and withstand further increases in the load, whenever the increase in displacement in the horizontal path does not exceed the maximum displacement allowed by the ductility of the structure the wall would not trigger a load redistribution at delamination. Therefore, the adjacent structural elements would not experience overload due to the delamination of the CFRP strips.

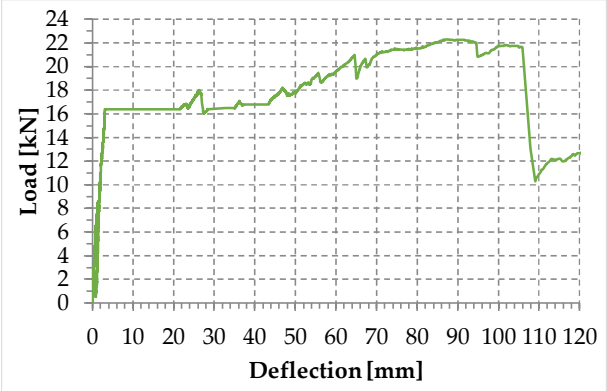

Figure 11. Load/deflection diagram for the first combined technique, in a hypothetical flexural test performed in the load control.

In conclusion, a greater number of transverse straps increases the delamination load and improve the load-bearing capacity after delamination (starting from the load of post-delamination), while a greater number of longitudinal straps decreases the load drop at delamination. A greater ribbons number also reduces the length of the horizontal path in Figure 11, so that the instantaneous deflection at the delamination can become compatible with the ductility of the structure.

2.2. Second Combined Technique: Straps Made of Steel Wire Ropes

 doi:10.20944/preprints201907.0340.v1

The combined technique with straps made of steel wire ropes (second combined technique) is an improvement of the combined technique discussed in Section 2.1 (first combined technique). The improvement consists in replacing the stainless steel ribbons with steel wire ropes, since the greater stiffness of the steel wire ropes will increase the frictional forces exerted at the interface between ropes and CFRP strips. As a result, the stiffness of the constraint established between two opposing CFRP strips will also increase, which will make the ideal I-beam stiffer. In conclusion, steel wire ropes should be more efficient than stainless steel ribbons in counteracting the out-of-plane displacements of a masonry wall subjected to hammering actions during a seismic event.

In the fastening system of the second combined technique, both loose ends of each steel wire rope form a Flemish eye (Figure 12a), which consists in turning the end back to form a loop and fixing the loose end back on the steel wire rope. A thimble installed inside the loop (Figure 12b) prevents the steel wire rope to bend too tightly when a device connected to the loop concentrates the load on a relatively small area. Furthermore, the thimble prevents the load from coming into direct contact with the steel wires, protecting the cable from pinching and abrading on the inside of the loop.

Figure 12. The fastening system of the second combined technique: (**a**) two Flemish eyes connected by an eye-eye turnbuckle and (**b**) detail of the thimble placed inside a Flemish eye.

In order to fix the loose end of the loop back to the steel wire rope it is possible to use either clips or ferrules, or a combination of the two (Section 3.4). Both the clips and the ferrules are useful for securing the loose ends of the steel wire ropes to avoid fraying, which is a very common occurrence in steel wire ropes.

The fastening system is completed with an eye-eye turnbuckle (Figure 12a), which closes the loop by connecting the two Flemish eyes of the same steel wire rope together. The turnbuckle is the device of the fastening system that allows us to tension the steel wire ropes. In fact, by rotating the metal frame of the eye-eye turnbuckle, the two threaded eyebolts screw in or out simultaneously without twisting the attached ends of the steel wire rope. This provides an adjustable pre-tension to the loop-shaped steel wire rope. Therefore, even the second combined technique is an active strengthening technique, which means that it does not require any damage to start working.

Lastly, if we choose to use stainless steel wire ropes for the straps, it is possible to avoid corrosion and compatibility problems as for the first combined technique.

Compared with the first combined technique, the second combined technique has the advantage of being adjustable. In fact, with the second combined technique it is possible to unlock and reposition the straps after a first tightening, without having to cut the steel wire ropes. It is also possible to adjust the tension in a steel wire rope after pre-tensioning an adjacent steel wire rope, which inevitably changes the stress in the previously tensioned steel wire rope. This makes the strapping process of the second combined technique more flexible than the strapping process of the first combined technique.

Section 3 will present the results of the first experimental program carried out at the LiSG laboratory of the University of Bologna on the second combined technique. As for Specimens W3 and W4 of the first combined technique (Section 2.1), the experimentation consisted in performing a three-point bending flexural test on a wall specimen strengthened with straps and CFRP strips on the two opposite faces of the masonry wall (Figure 13), to obtain an I-beam behavior from the mechanical coupling between the two techniques. For comparison purposes, the materials and dimensions of the

Preprints (www.preprints.org) | NOT PEER-REVIEWED | Posted: 30 July 2019 doi:10.20944/preprints201907.0340.v1

masonry wall and the layout of the straps are the same as those used for the first combined technique (Figure 13). In particular, the holes follow the quincunx pattern—as for Specimens W3 and W4 (Section 2.1)—and belong to intersecting three-dimensional nets.

Some straps of both three-dimensional nets tie together the CFRP strips of the opposite faces, along the vertical centerlines.

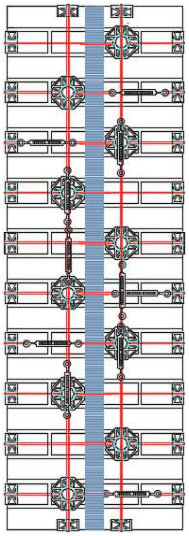

Figure 13. Arrangement of the steel wire ropes in the second combined technique.

For the strapping scheme shown in Figure 13, the horizontal straps that pass over the CFRP strips are longer than the horizontal straps that only pass over bricks. The eye-eye turnbuckles of the longer horizontal straps alternate in position on the front and back face, in order to obtain a sort of strapping symmetry on the two faces. This is useful for minimizing non-symmetrical behaviors and torsional effects induced on the specimen by the strapping system, during the test.

The eye-eye turnbuckles of the shorter horizontal straps are too long to lie on the two main faces. However, they find an optimal positioning on the lateral faces of the masonry wall, which is a two-headed wall (Figure 14), with the bricks that measure 24.5 cm in length, 5.5 cm in height, and 11 cm in depth (Bolognese type). As the planned dimensions of the brick wall are 50 × 146 × 23 cm, the geometric features of the Bolognese bricks do not exactly fit the length of the wall. Therefore, it was necessary to shorten the end bricks of the odd rows in Figure 15 to obtain the desired length.

Figure 14. The fastening system of the second combined technique: detail of the clamping system positioned along the lateral face of the brick wall (23 cm).

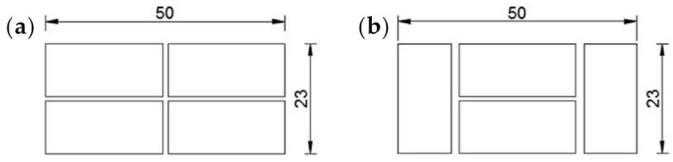

Figure 15. Arrangement of the bricks in the rows (all measures in *cm*): (**a**) odd rows; (**b**) even rows [1].

Preprints (www.preprints.org) | NOT PEER-REVIEWED | Posted: 30 July 2019 doi:10.20944/preprints201907.0340.v1

3. Experimental Program

3.1. Bricks and Mortar

The bricks and mortar of the experimental program are the same as those of the experimentation on the first combined technique [1]. Their mechanical characterizations complied with UNI EN 772-1 and UNI EN 1015-11/2007, respectively. In particular, UNI EN 772-1 establishes to perform uniaxial compression tests on 6 brick specimens, while UNI EN 1015-11/2007 establishes to perform three-point bending flexural tests on 6 prismatic specimens and uniaxial compression tests on 12 cubic specimens obtained by the prismatic specimens after the flexural tests.

Table 1 collects the results of the mechanical characterization on the bricks of the experimentation, while Table 2 shows the results of the mechanical characterization on the mortar. As can be easily checked in Table 2, the mortar of the experimental program is of the M20 type.

Table 1. Geometric and mechanical characteristics of the six brick specimens [1].

Specimen	Dimensions [mm]	Weight [g]	Breaking Load [N]	Compressive Strength [N/mm²]	Normalized Compressive Strength [N/mm²]
PA1	55 × 54 × 55	296.1	116436	39.63165	34.47953
PA2	57 × 57 × 55	317.8	165730	50.91128	44.29281
PB1	55 × 53 × 55	297.5	146733	49.62439	43.17322
PB2	56 × 55 × 57	319.2	142681	46.09916	40.10627
PC1	56 × 53 × 56	310.5	144933	47.77687	41.56587
PC2	56 × 55 × 56	317.1	149422	48.14767	41.88848

Table 2. Geometric and mechanical characteristics of the mortar specimens [1].

Specimens of the Flexural Tests	Dimensions [mm]	Weight [g]	Breaking Load in Bending [N]	Flexural Strength [N/mm²]	Specimens of the Compression Tests	Breaking Load in Compression [N]	Compressive Strength [N/mm²]
P1	40 × 40 × 160	466.42	1758	4.12	P1A	30530	19.08
					P1B	36730	22.96
P2	40 × 40 × 160	469.81	1838	4.31	P2A	30980	19.36
					P2B	30930	19.33
P3	40 × 40 × 160	470.42	1443	3.38	P3A	27500	17.19
					P3B	28530	17.83
P4	40 × 40 × 160	459.63	1885	4.42	P4A	34544	21.59
					P4B	27730	17.33
P5	40 × 40 × 160	463.81	1990	4.66	P5A	33880	21.18
					P5B	35200	22.00
P6	40 × 40 × 160	462.01	1598	3.75	P6A	30400	19.00
					P6B	30450	19.03

3.2. Protective Funnel-Shaped Plates and Rounded Angles

At the corners of the straps, the second combined technique uses the same protective elements as those of the first combined technique [1]: the 3D printed funnel-shaped plates and rounded angles shown in Figure 16.

3D printing allows us to overcome some intrinsic geometric limits of the traditional hot forming technique, used for the funnel-shaped plates and rounded angles of the CAM system [1]. The choice of the material and the optimization of the shape of the 3D printed protective elements are part of the experimental program conducted at the LiSG laboratory of the University of Bologna. As already

 doi:10.20944/preprints201907.0340.v1

specified in Reference [1], the final choice as far as the material is concerned fell on the PLA (Polylactic Acid) filament, a thermoplastic, biodegradable, and non-toxic polyester used in FDM (Fused Deposition Modeling) 3D printing, because the PLA filament is one of the most eco-friendly 3D printer materials available. Both the plates and angles have rounded external corners (the parts in contact with the straps) and internal corners at 90° (the parts in contact with the wall edges). Moreover, the flat parts of the 3D printed protective elements have a truss shape that allows the mortar to fill the truss structure, in order to improve the adherence between the masonry wall and the protective elements once the mortar has hardened (Figure 17).

Although PLA degrades in an exposed natural environment, when adequately protected against degradation its stiffness and hardness make it similar to iron. It is worth noting that the damage to the protective elements after the experimental tests on the first combined technique was actually so low as to allow the reuse of the protective elements for the bending test on the second combined technique.

The second combined technique also requires some small pieces of steel ribbons to protect the rounded corners of the 3D printed elements, as shown in Figure 17. In fact, the small cross-section of the steel wire ropes tends to indent the rounded corners of the 3D printed elements when it is in direct contact with them.

Figure 16. 3D printed funnel-shaped plates and rounded angles.

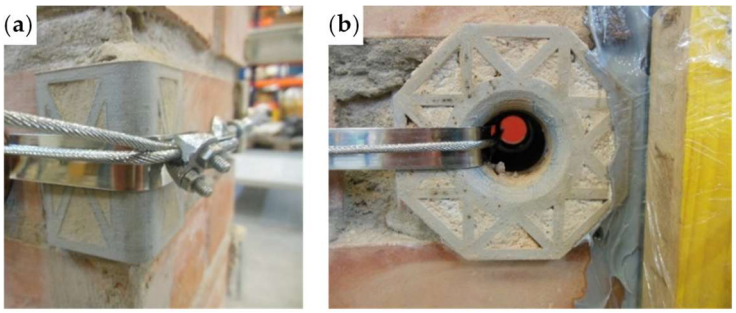

Figure 17. The pieces of steel ribbons positioned under the steel wire ropes at the corners of the protective elements: details of (**a**) a rounded angle and (**b**) a funnel-shaped plate.

3.3. Mechanical Characterization of the Steel Wire Ropes

A steel wire rope is a set of steel wires rolled into a spiral. Compared with wrought iron chains, which have recorded a record of mechanical failures since many catastrophic failures have occurred due to flaws in chain links or solid steel bars, the steel wire ropes have a less brittle behavior. In fact, any flaws in the wires that make up a steel cable are less critical as the other wires easily take up the load. Furthermore, the friction between the individual wires and strands helps to compensate for minor failures in the short-term. However, in the long-term, friction is the main cause of rope wear.

Due to a higher carbon content in the composition, when compared with structural steels the steel wire strength is significantly high. However, the ductility of the steel wire is lower than that of the structural steel [42]. In fact, usually the strain at breaking of the steel wire is about one-sixth of that corresponding to a mild steel. Furthermore, the simple helical and the spiral strand have lower elasticity modulus than a common wire. Despite the lower-elasticity modulus, helical strands have the advantage of the self-compacting with the tensioning, not requiring wrapping.

 doi:10.20944/preprints201907.0340.v1

According to EN 1993-1-11, the steel wire ropes of the experimentation are, more precisely, spiral strand ropes, built with independent layers of helically arranged round wires (Figure 18). The choice fell on spiral strand ropes, as a rope formed by a single strand of thick wires without a core will be rigid and resistant to wear and corrosion [42]. Its properties are suitable for static, immobile applications, such as supports, braces, edge ropes, and struts, usually used in tensile structures and fixed textile construction.

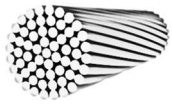

Figure 18. The cross-section of a spiral strand rope, as defined in EN 1993-1-11.

ASTM A-931 covers the tensile testing of steel wire ropes and strands at room temperature. The purpose of the test is to determine the breaking force, yield strength, elongation and modulus of elasticity.

Figure 19 shows the experimental set-up of the tensile test performed on one spiral strand rope of the experimentation. As usual for steel ropes, an LVDT (Linear Variable Differential Transformer) measured the crosshead displacement to obtain the extension of the specimen (Figure 19). In fact, due to high-energy specimen failures, using a traditional contacting extensometer there is a risk of damaging and/or transforming the extensometer into a projectile. To avoid this, it is necessary to remove the extensometer prior to specimen failure. However, since the specimen will be under load, this entails a significant risk for the operator, as there is the possibility that the specimen will break during the removal of the extensometer.

Figure 19. Positioning the LVDT to measure the displacement of the crosshead.

Furthermore, if the extensometer remains attached to the sample, reduction in rope diameter due to Poisson effect and twisting can cause the contact points to slip or the device to fall off. It could also happen that the edges of the knife cause stress concentrations, resulting in premature failure.

Figure 20 shows the load/displacement diagram of the tested specimen, while Figure 21 shows the specimen after failure. The load drop in Figure 20 for a displacement of almost 3.9 *mm* corresponds to the moment in which the steel wire rope began to fray. The fraying occurred at one end of the specimen (right end in Figure 21a,c), while on the other end the individual steel wires of the specimen twisted (left end in Figure 21a,b). Each load drop in Figure 20 occurred due to the failure of one or more fraying steel wires. The first load drop did not immediately bring the sample to failure and further load increases were possible after it, as the remaining steel wires took up the load. A similar load redistribution occurred after each steel wire failure. This allowed the specimen to reach

 doi:10.20944/preprints201907.0340.v1

a final displacement equal to about 182% of the displacement of first fraying, with an average residual load during the fraying that is about 52% of the maximum load.

For comparison purposes, the selection criterion for the cross-section of the steel wire rope was to choose a steel wire rope with the same yield load as that of the steel ribbons used in the experimental program on the first combined technique [1]. The yield load in Figure 20 is actually comparable to the yield load of the steel ribbons of Reference [1] (Figure 22). The specimen failure took place at the frayed end, with a final displacement equal to about 8.6% of the final displacement for the steel ribbons of Reference [1] (Figure 22).

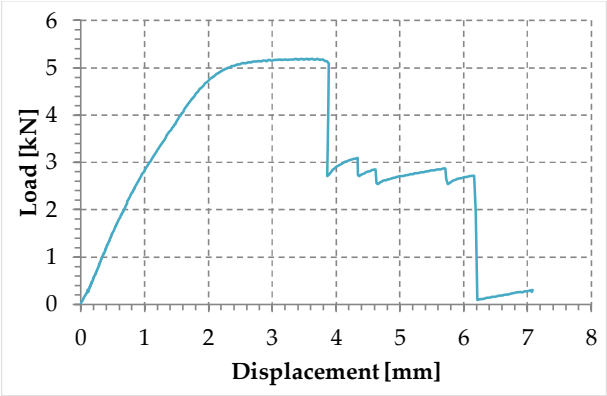

Figure 20. Load/displacement diagram of the steel wire rope used in the experimentation.

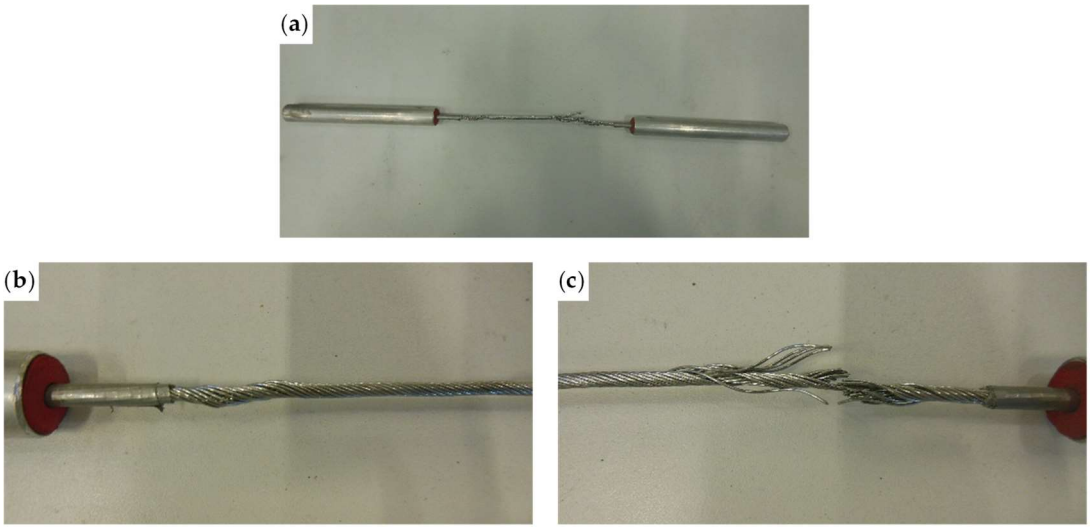

Figure 21. The spiral strand rope after the test: (**a**) general overview, (**b**) detail of wire twisting at the left end, and (**c**) detail of the failure due to fraying, at the right end.

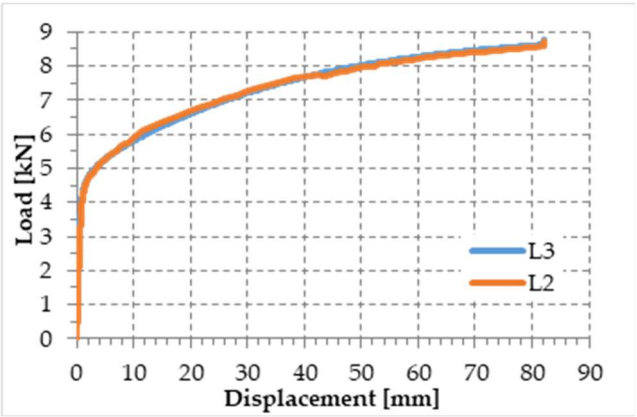

Figure 22. Load/displacement diagrams for the steel ribbons used in Reference [1].

3.4. Mechanical Characterization of the Jionts

As already mentioned in Section 2.2, the most common devices for fixing the loose end of a Flemish eye back to the steel wire rope are ferrules and clips.

Ferrules—also often referred to as eyelets or grommets—are narrow circular clamps made from metal (Figure 23). They are useful to hold together and connect steel wires, generally by crimping, swaging, or otherwise deforming the ferrule to tighten it permanently on the parts it holds.

A clip is a steel wire rope clamp that consists of a U-shaped bolt, a forged saddle, and two nuts (Figure 24a). The saddle includes two holes to fit to the U-bolt and the nuts secure the arrangement in place (Figure 24b).

Figure 23. The ferrules of the experimentation: (**a**) longitudinal dimension, (**b**) transversal dimension, and (**c**) thickness.

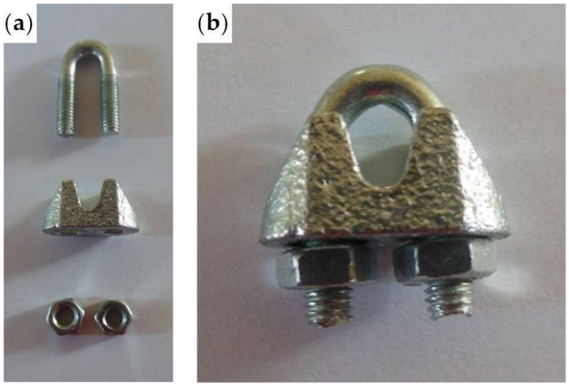

Figure 24. The clips of the experimentation: (**a**) constituent parts and (**b**) a clip after assembly.

The loose end and the steel wire rope on which to fix it pass in the space between the U-bolt and the saddle, placed one on the other on the saddle (Figure 25). By screwing the nuts, the U-bolt and the saddle approach each other, holding the two parts of the steel wire rope together.

The flat bearing seat and extended prongs of a saddle protect the load-bearing end of the rope against crushing and abuse. For this purpose, the saddle portion of the clamp assembly must lie against the load-bearing or "live" side (Figure 25), not against the non-load-bearing or "dead" side of the cable.

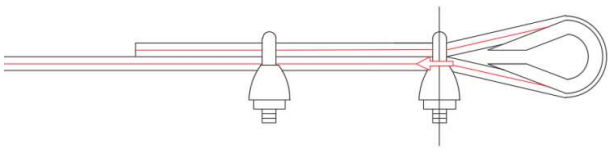

Figure 25. Eccentricity of the load provided by a clip to the steel wire rope, with respect to the Flemish eye.

One of the aims of the experimental program was to analyze various possible methods to close the Flemish eyes, in order to identify the best performing joint. Actually, the strength of a strap with

 doi:10.20944/preprints201907.0340.v1

a junction is always lower than the strength of the strap alone. The methods of closure of the Flemish eyes taken into consideration consist in using:

- 1 ferrule (Specimen 1, Figure 26);
- 2 ferrules in succession (Specimen 2, Figure 27);
- 1 clip (Specimen 3, Figure 28);
- 2 clips in succession (Specimen 4, Figure 29);
- 1 ferrule and 2 clips, in succession, starting from the Flemish eye (Specimen 5, Figure 30);
- 1 ferrule, 1 clip, a second ferrule, and a second clip, in succession, starting from the Flemish eye (Specimen 6, Figure 31);

The thimbles used to preserve the natural shape of the Flemish eyes for the specimens listed above have the geometrical characteristics shown in Figure 32.

Figure 26. Specimen 1: Flemish eye closed by 1 ferrule.

Figure 27. Specimen 2: Flemish eye closed by 2 ferrules.

Figure 28. Specimen 3: Flemish eye closed by 1 clip.

Preprints (www.preprints.org) | NOT PEER-REVIEWED | Posted: 30 July 2019 doi:10.20944/preprints201907.0340.v1

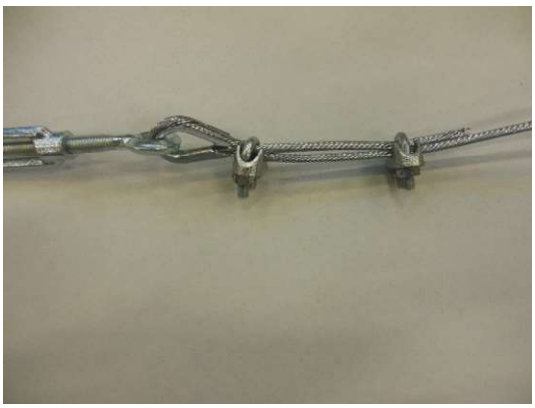

Figure 29. Specimen 4: Flemish eye closed by 2 clips.

Figure 30. Specimen 5: Flemish eye closed by 1 ferrule and 2 clips, in succession.

Figure 31. Specimen 6: Flemish eye closed by 1 ferrule, 1 clip, 1 ferrule, and 1 clip, in succession.

Figure 32. The thimbles of the experimentation: (**a**) overview, (**b**) thickness, and (**c**) longitudinal dimension.

 doi:10.20944/preprints201907.0340.v1

Specimens 1 and 2 had a very bad behavior, because they failed for a load value much lower than the maximum load of the steel wire rope without a joint (Table 3). Moreover, both specimens showed an excessive deformation of the Flemish eyes, which squashed despite the use of the thimble. However, since the maximum load of Specimen 2 was more than double the maximum load of Specimen 1 (Table 3), the use of a second ferrule helps the joint to withstand higher loads.

Table 3. Maximum loads of the steel wire rope and the six jointed specimens.

Specimen	Maximum Load [kN]
Without a joint	5.186
Specimen 1	1.100
Specimen 2	2.570
Specimen 3	4.139
Specimen 4	4.447
Specimen 5	4.974
Specimen 6	4.655

Figure 33 shows the comparison between the load/displacement diagrams of the steel wire rope without a joint and the four specimens with Flemish eyes closed by means of clips or combinations between clips and ferrules. In particular:

- The load of Specimen 3 increased linearly up to a value of about 2.4 kN. Then, the slope of the load/displacement diagram decreased due to the yield behavior of the steel wires and the load continued to increase monotonically up to a value of about 2.9 kN. At this point, the specimen suffered a load drop due to the squashing of the Flemish eyes. Once the squashing of the Flemish eyes was over, the load started to rise again, up to its maximum value. Afterwards, the fraying of the steel wires quickly led the specimen to failure. It is worth noting that the fraying has started from one of the two clips used to close the Flemish eyes (Figure 34). In fact, the eccentricity of the load supplied to the steel wire rope—due to the non-perfect coaxiality between the turnbuckle and the "live" side—brought the flat bearing seat of the clip to rotate, until its edge came into direct contact with the steel wires. This caused pinching and abrading of the steel wires and, consequently, their failures in rapid succession.
- The linear behavior of the load/displacement diagram of Specimen 4 terminated for a load value of about 3.4 KN, which corresponds to approximately 142% of the load at the end of the linear branch of Specimen 1. The yield behavior of the steel wires and squashing of the thimbles took place simultaneously from this moment forward, decreasing the slope of the load/displacement diagram but without causing any load drop. The slope of the linear branch is greater than the slope of the linear branch for Specimen 3, which means that Specimen 4 is stiffer than Specimen 3. Actually, the stiffness of Specimen 4 is comparable to the stiffness of the steel wire rope without a joint. The yield behavior and squashing processes terminated with the fraying of the steel wires, which is responsible for the "step behavior" of the last part of the load/displacement diagram: each load drop in this final part of the diagram is the consequence of the failure of one or more steel wires. The fraying started from a clip, the first from the Flemish eye (Figure 35). As for Specimen 3, the cause for this lies in the non-perfect coaxiality between the turnbuckle and the live end (Figure 25). However, the second clip—that forces the part of the "dead" side between the two clips to bear load—partially eliminates the torsion of the first clip, delaying the fraying. This could also be the reason for the greater stiffness and maximum load of Specimen 4.

Preprints (www.preprints.org) | NOT PEER-REVIEWED | Posted: 30 July 2019 doi:10.20944/preprints201907.0340.v1

- The purpose of the fifth fastening scheme was to eliminate the torsion of the first clip of the fourth fastening scheme, that is, the clip closest to the Flemish eye. In other words, the function of the ferrule was to center the load on the two clips (Figure 36). Specimen 5 did not actually fray near the first clip (Figure 37): it frayed near the second clip. The improved load centering allowed the specimen to withstand a higher ultimate load, comparable to the ultimate load of the steel wire rope without a joint. However, the ferrule caused an excessive deformation of the Flemish eyes, as for Specimens 1 and 2. This greatly reduced the stiffness of the specimen.
- The sixth fastening scheme introduces an additional ferrule between the two clips to eliminate even the rotation of the second clip, with the aim of preventing the specimen from fraying near both clips. The second ferrule actually further improved the load centering, eliminating fraying near both clips. However, this concentrated the deformation phenomena on the thimble that twisted, cutting off the steel wires (Figure 38). The twisting of the thimble occurred due to the excessive squashing of the Flemish eye. In fact, once the two ends of the thimble come into contact, the further squashing of the Flemish eye is possible only by forcing the two ends of the thimble to slide one over the other in the direction orthogonal to the load. This causes the twisting borders of the thimble to cut the steel wires. Also in Specimen 5 the excessive deformation of the Flemish eye caused a twist of the thimble (Figure 35), but this did not lead to damage to the steel wires. Lastly, the concentration of the deformations on the Flemish eyes greatly reduced the stiffness of the specimen, as for Specimen 5: Specimen 6 and Specimen 5 have practically the same stiffness.

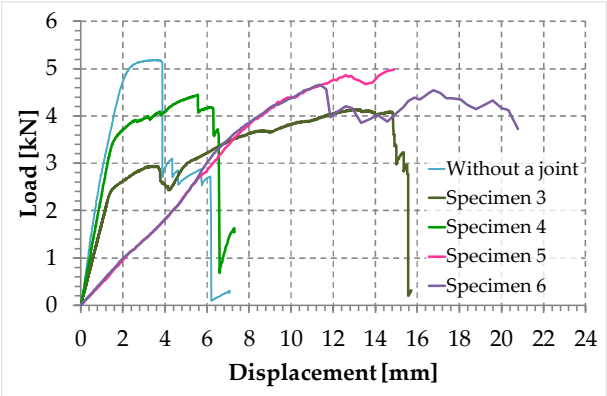

Figure 33. Load/displacement diagrams for 5 of the 7 specimens used for the mechanical characterization of the joints.

Figure 34. Failure mechanism of Specimen 3.

In conclusion, it seems that the clips allow a certain degree of sliding between the two sides of a steel wire rope, while the ferrules are much more effective in counteracting the sliding. The sliding

 doi:10.20944/preprints201907.0340.v1

allowed by a clip is the main responsible for the rotation of the clip and the consequent fraying of the steel wires that came into contact with the edge of its flat bearing seat. On the other hand, however, the elimination of the sliding by means of a ferrule causes exaggerated deformations of the Flemish eyes, which diminish the stiffness of the fastening system. The fastening system chosen for the next phase of the experimentation is the fourth fastening scheme (Figure 29) because, for the purposes of experimentation, the fastening system must be as stiff as possible.

Figure 35. Failure mechanism of Specimen 4.

Figure 36. How the ferrule modifies the load centering on the two clips, compared with the load transfer scheme of Figure 25.

Figure 37. Failure mechanism of Specimen 5.

Figure 38. Failure mechanism of Specimen 6.

 doi:10.20944/preprints201907.0340.v1

3.5. Three-Point Bending Flexural Test on a Masonry Specimen

3.5.1. Preparation of the Specimen and Test Setup

In order to evaluate the effectiveness of the second combined technique to restore a damaged structural element, the wall specimen used in the experimentation is a specimen already tested in the experimental program on the first combined technique. In particular, the specimen of the first experimentation used for the second experimentation is Specimen W1 of Reference [1], a drilled masonry wall with the holes arranged in quincunxes, tested under three-point bending load after strapping by means of two staggered three-dimensional nets of straps made of steel ribbons.

During the three-point bending test on Specimen W1, an inner hinge opened near the middle cross-section (11th mortar bed joint from the left, in Figure 39a). The disconnection along the failed mortar bed joint led the left and right parts of the specimen to rotate around the inner hinge (center of relative rotation) in a controlled manner, since the high ductility of the steel ribbons (Figure 22) allowed the disconnection to open up considerably (Figure 39), without ever causing loss of equilibrium. No straps broke during the opening of the disconnection. However, of the two longitudinal straps that crossed the disconnection, the one that passed through the hole closest to the inner hinge broke the protective funnel-shaped element and ripped off the thin layer of brick located between the disconnection and the cavity for the passage of the straps (Figure 39b).

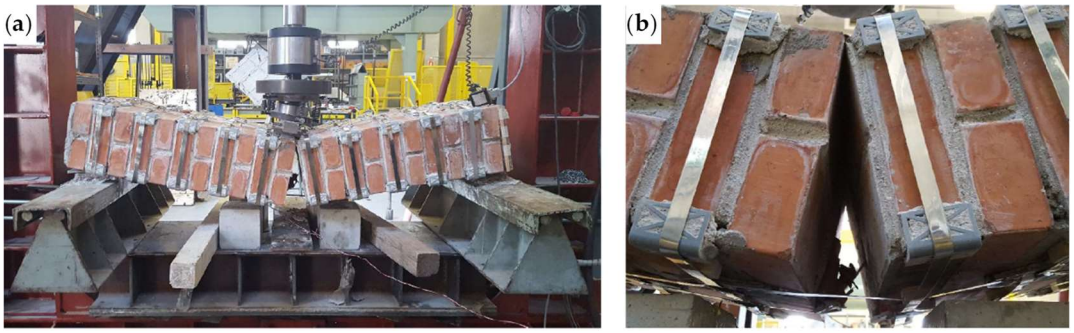

Figure 39. Specimen W1 at the end of the flexural test [1]: (**a**) overview of the disconnection mechanism and (**b**) detail of the disconnected cross-section: brick tear in the background.

The preparation of the wall specimen took place as follows:

- Removal of Specimen W1 from the testing machine;
- Removal of all the straps from Specimen W1;
- Removal of the mortar from the disconnected cross-section of Specimen W1 (11th mortar bed joint from the left, in Figure 39a), where the crack propagation occurred in Mode I [43–45] (opening mode in Figure 40);
- Overturning in the vertical configuration of the two parts resulting from the failure of Specimen W1;
- Restoration of the cavity for the passage of the straps near the disconnected cross-section, inserting a steel tube of the same external diameter as the drilled holes;
- Lifting and holding of the upper part of Specimen W1 in position, by means of a girder crane;
- Restoration of the disconnected mortar bed joint of Specimen W1 (Figure 41a);
- Curing of the mortar on the restored cross-section;
- Application of longitudinal CFRP strips 50 mm wide and 1.2 mm thick, on both main faces of the restored specimen (Figure 41b);
- Application of the straps on the restored specimen, according to the scheme of Figure 42.

The length of the fastening system made it impossible to pass the vertical loops in Figure 42 through adjacent holes. This made it necessary to use the holes alternately along the vertical direction. In order not to leave any unused holes, the vertical loops were stagger along the vertical direction,

Preprints (www.preprints.org) | NOT PEER-REVIEWED | Posted: 30 July 2019 doi:10.20944/preprints201907.0340.v1

giving rise to the four staggered meshes (a, b, c, and d) in Figure 42. Furthermore, the number of steel wire ropes for the central vertical loops of meshes b and d were increased from 1 to 2 (Figure 42).

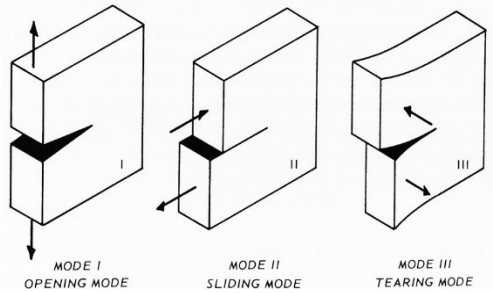

Figure 40. The three modes of failure in fracture mechanics.

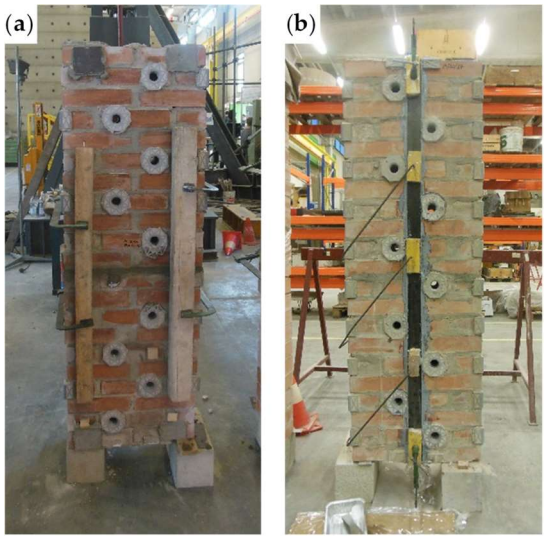

Figure 41. Preparation of the specimen: (**a**) restoration of the 11th mortar bed joint from above (front view) and (**b**) application of the CFRP strips after curing of the restored mortar bed joint (back view).

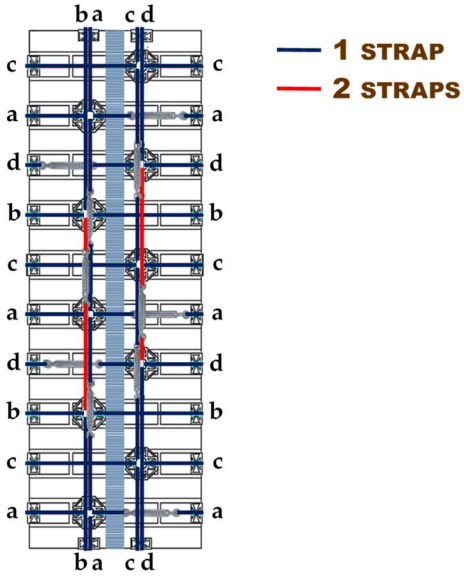

Figure 42. The four staggered meshes to strap the restored specimen (Specimen W5).

The strapping took place in two stages—as for the first combined technique—first arranging all the straps parallel to the shorter side (transverse straps) and, secondly, completing the strapping with the straps parallel to the longer side (longitudinal straps). This allows the longitudinal straps to pass

Preprints (www.preprints.org) | NOT PEER-REVIEWED | Posted: 30 July 2019 doi:10.20944/preprints201907.0340.v1

over the transverse straps at the intersections between the straps (Figure 43c). As a result, the pre-tension of the longitudinal straps pushes the transverse straps against the wall, which allows the transverse straps to load the CFPR strips symmetrically, according to schemes a) and b) of Figure 43, alternatively. This is essential to couple the steel straps and the CFRP strips mechanically, as the frictional forces from contact help to establish the I-beam behavior described in Section 1.

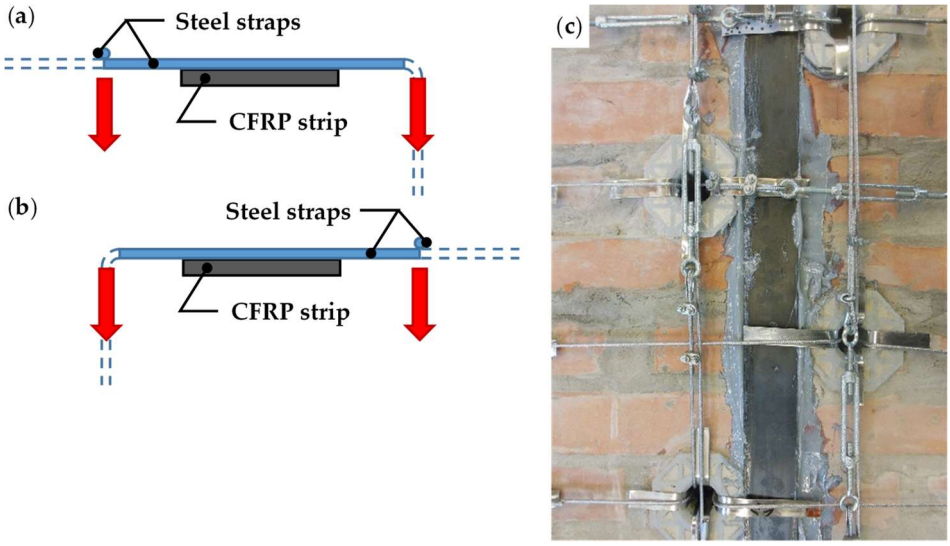

Figure 43. Intersections between longitudinal and transverse straps: (**a**) the longitudinal strap pushes down on the transverse strap to the left of the CFRP strip (cross-section view, not to scale). (**b**) The longitudinal strap pushes down on the transverse strap to the right of the CFRP strip (cross-section view, not to scale). (**c**) Detail of strap arrangement, with scheme sequence a, b, a, b.

The new label of Specimen W1 after restoration and strengthening by means of the second combined technique is “Specimen W5”.

Since the loading piston of the testing machine applies the load vertically, it was necessary to overturn Specimen W5 in the horizontal configuration. This required slinging the specimen as shown in Figure 44, to allow the girder crane to hook, lift, and overturn the masonry wall.

The slings also had the function of tying a wooden “stretcher” on the front side of the masonry wall (Figure 44a), to avoid damage to the specimen during the subsequent handling phase. Some wooden spacers between the wooden “stretcher” and the masonry wall (Figure 44b) prevented the wooden "stretcher" from coming into direct contact with the straps. In fact, in the absence of spacers, the wooden “stretcher” could crush the straps when the slings push it against the wall, damaging the three-dimensional tying system.

The overturning led to placing the wooden "stretcher" on the lower side of the specimen (Figure 45a). Furthermore, the girder crane overturned Specimen W5 on two wooden beams positioned along the shorter sides of the specimen, near the ends (Figure 45a), so as to leave some space under the specimen to allow the passage of the forklift forks (Figure 45b). When the forklift lifted Specimen W5 to place it on the testing machine, the stiffness of the wooden "stretcher" prevented the specimen from bending.

In order to distribute the load given by the loading piston, it was necessary to place some flat steel bars on the central cross-sections of the specimens (Figure 46). The arrangement of the flat steel bars allowed the load not to compress the straps and the upper CFRP strip.

The flat steel bar system in Figure 46 is stiff enough to provide a uniform load on the contact areas. However, the stress field induced in the specimen may not be as desired. In fact, recent experimental and analytical studies on static contact [46–50] do not allow us to exclude the existence of perturbative effects that do not depend on the stiffness of the loading system. As the perturbative effects concentrate along the contours of the contact areas, they can be responsible for some local damage near the contact areas.

 doi:10.20944/preprints201907.0340.v1

During the test, some Linear LVDTs acquired the displacements at the ends and the middle point on the lower faces.

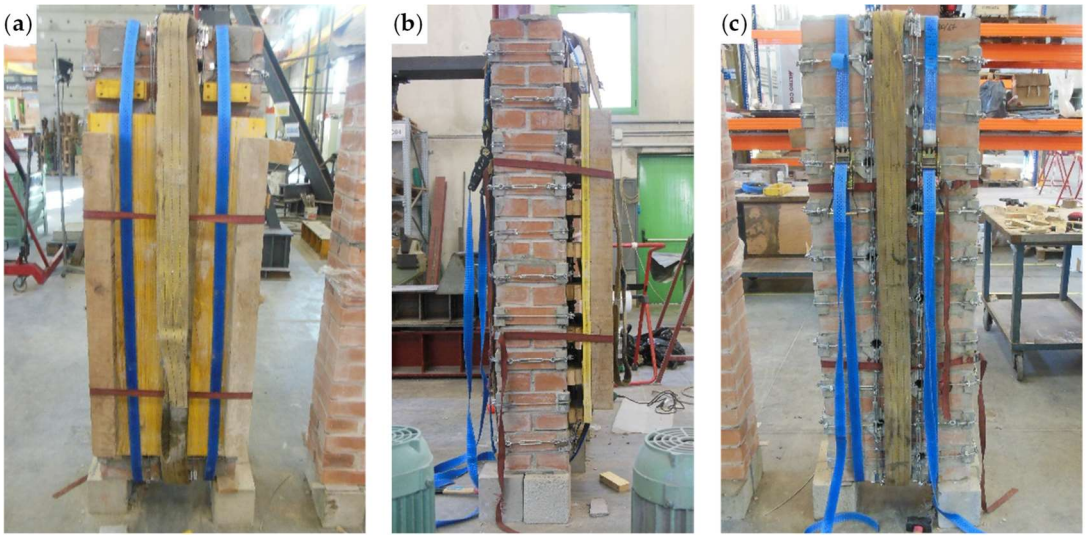

Figure 44. Slinging of Specimen W5, used to allow handling and overturning of the specimen by means of the girder crane: (**a**) front view, (**b**) viewed from the left, and (**c**) back view.

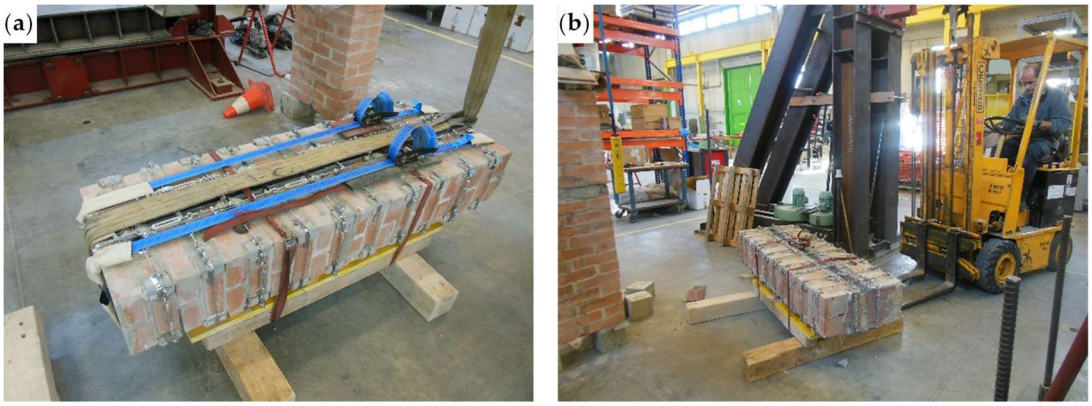

Figure 45. Handling of Specimen W5: (**a**) overturning of the specimen on the wooden beams, with the wooden "stretcher" placed below and (**b**) positioning the forklift forks to lift the specimen.

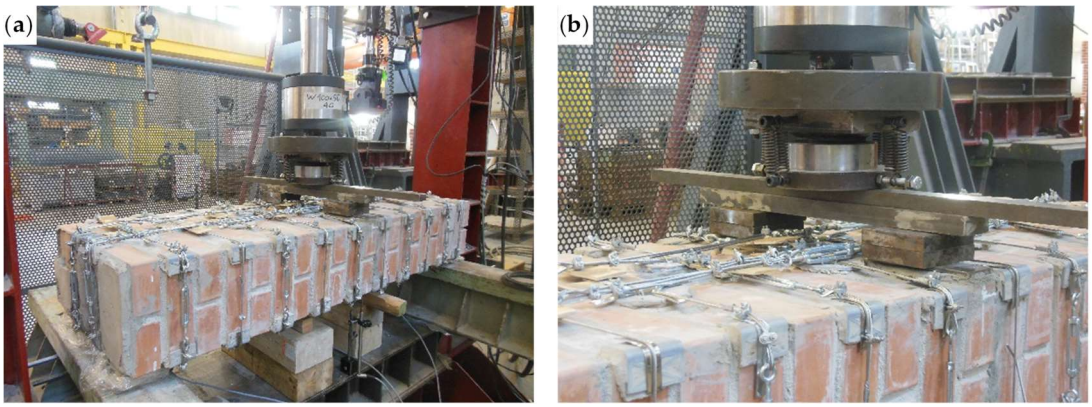

Figure 46. The flat steel bars for load distribution on the middle cross-section: (**a**) overview of the loading system and (**b**) detail of the passage of the steel wire ropes under the loading piston.

3.5.2. Results and Discussion

The three-point bending flexural test took place under displacement control. The behavior of the specimen was highly ductile, as for the specimens strengthened with the first combined technique

Preprints (www.preprints.org) | NOT PEER-REVIEWED | Posted: 30 July 2019 doi:10.20944/preprints201907.0340.v1

(Sections 2.1 and 3.5.1). In fact, even in this latter case the specimen did not undergo an actual collapse because the steel wire ropes allowed the inner hinge to provide relative rotations in a controlled manner, preventing the specimen from falling (Figure 47a). However, contrary to what happened with the first combined technique (Section 3.5.1), several longitudinal straps suffered fraying and failure during the test, in particular those positioned on the middle cross-section (Figure 47b). This occurred due to the lower ductility of the steel wire ropes compared to the steel ribbons of the first combined technique (Section 3.3). In addition, one of the two threaded eyebolts of a defective turnbuckle positioned near the middle cross-section has opened, due to the high load supplied by the steel wire rope. This led the Flemish eye to come out of the threaded eyebolt, interrupting the continuity of the strap (Figure 47b and Figure 48b).

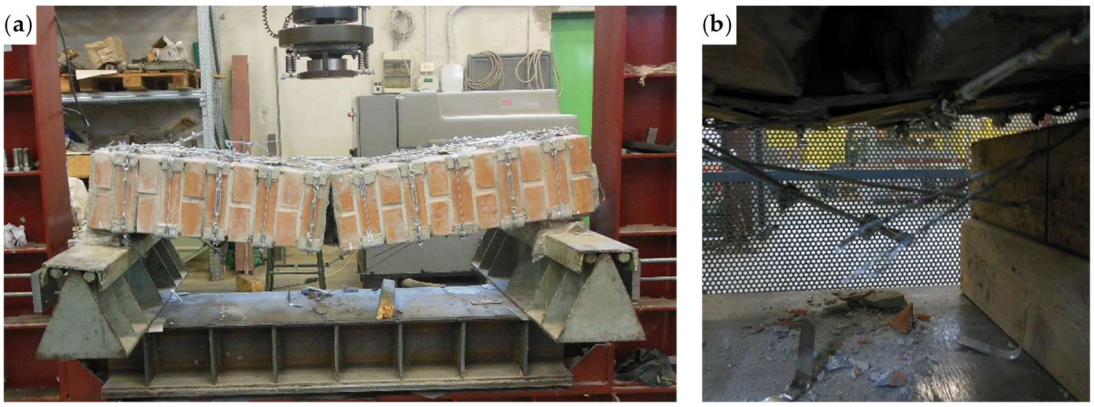

Figure 47.: The specimen on the testing machine after the test: (**a**) front view and (**b**) detail of the broken straps under the middle cross-section (back view).

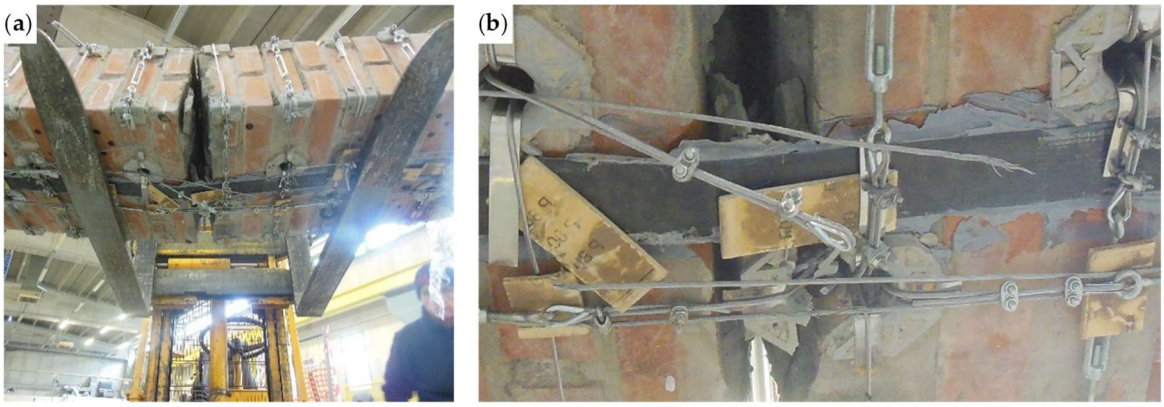

Figure 48.: The specimen on the forklift after the test: (**a**) bottom/back view (the vertical white marks indicate the middle cross-section) and (**b**) detail of the disconnected cross-section viewed from below, with the Flemish eye that came out of the threaded eyebolt in the foreground.

The view from below in Figure 48b also shows a broken funnel-shaped plate near the middle cross-section. Since the internal disconnection of Specimen W5 opened in the same position as for Specimen W1 (Specimen W5 before the restoration), also for Specimen W1 the funnel-shaped plate near the middle cross-section broke into two parts. In Specimen W5, however, the failure of the funnel-shaped plate did not entail the interruption of the chain made by the longitudinal straps (Figure 48b), since the steel tube inserted to restore the passage of the straps (Section 3.5.1) prevented the longitudinal strap on the left of Figure 48b from tearing the brick.

The internal disconnection opened on the 11th mortar bed joint from the right of Figure 47a, which is precisely the restored mortar bed joint, as already mentioned. However, the maximum load of Specimen W5 is much higher than the maximum load of the same specimen before the restoration (Specimen W1): to be precise, it is 479% of the maximum load reached before the restoration (Figure 49). Therefore, the use of steel wire ropes instead of steel ribbons provided a successful restoration.

Preprints (www.preprints.org) | NOT PEER-REVIEWED | Posted: 30 July 2019 doi:10.20944/preprints201907.0340.v1

The disconnection along the 11th mortar bed joint occurred for a load value of about 23 kN. This disconnection did not result in any appreciable load drop in the load/deflection diagram of Specimen W5, but led to a slight decrease in the slope of the diagram (Figure 49). Moreover, the disconnection was not appreciable to the naked eye, at first, since the straps took up the load no longer supported by the failed mortar, not allowing the disconnection to open. This increased the load on the longitudinal straps positioned above the disconnected cross-section. As a result, some steel wire ropes began to fray. The four load drops observed in the load/deflection diagram of Specimen W5 for the load values of about 27.122 kN, 29.520 kN, 31.698 kN, and 34.444 kN occurred precisely because of the fraying (Figure 49b). After each of these load drops, the load started to rise again, exceeding the load reached before fraying. Furthermore, the first load drop made the disconnection visible along the 11th mortar bed joint (Figure 50).

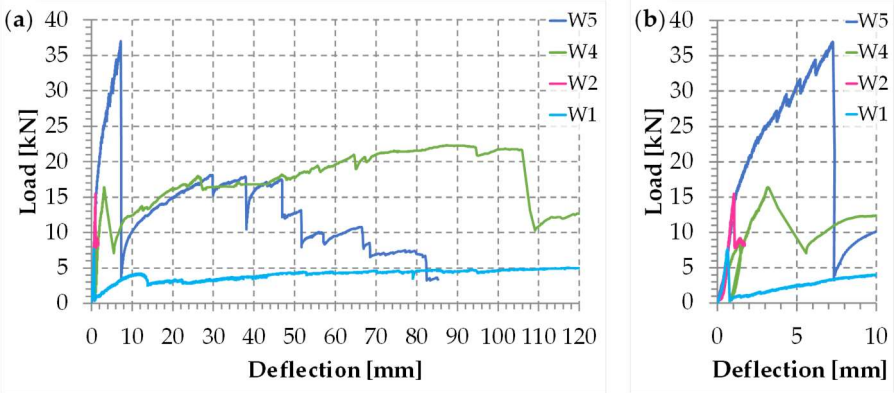

Figure 49. Comparison between the load/deflection diagrams of the specimens reinforced with CAM-like ribbons (Specimen W1), CFRP strips (Specimen W2), first combined technique (Specimen W4), and second combined technique (Specimen W5): (**a**) complete diagrams up to the end of the tests and (**b**) detail of the peak of delamination of Specimen W5, with a magnified scale factor for the deflection axis.

Figure 50. A snapshot of when the disconnection became visible for the first time (load value of about 27.122 kN), on the right of the middle cross-section: the stiffness of the longitudinal straps does not allow free rotation around the inner hinge (back view, the vertical white marks indicate the middle cross-section).

Preprints (www.preprints.org) | NOT PEER-REVIEWED | Posted: 30 July 2019 doi:10.20944/preprints201907.0340.v1

At the load value of 36.992 kN (maximum load), a fifth load drop occurred (Figure 49). This additional load drop has a different cause than the previous ones, as it is the consequence of the delamination of both CFRP strips. It is worth noting that the delamination load of Specimen W5 is about 239% of the delamination load of the specimen strengthened only by the CFRP strips (Specimen W2 of Reference [1], see Figure 49). This is a significant improvement compared to the first combined technique (Specimen W4 of Reference [1], see Figure 49), which provided a delamination load equal to 106% of the delamination load of Specimen W2. The improvement also concerned the ductility up to delamination of the specimen reinforced with the second combined technique: the delamination deflection of Specimen W5 is approximately 242% of the delamination deflection of Specimen W4 and 743% of the delamination deflection of Specimen W2.

The second combined technique is more performant than the first combined technique also as far as the stiffness of pre-delamination is concerned. In particular, it is worth noting that the stiffness of Specimen W5 is comparable to the stiffness of Specimen W2 up to the delamination load of Specimen W2 (Figure 49b). Specimen W4, on the contrary, suffered a decrease in stiffness starting from a load value equal to about 30% of the delamination load of Specimen W2 (Figure 49b).

Since buckling is the main cause of delamination for the upper CFRP strip, the detachment of the upper CFRP strip occurred in Mode I (Figure 40), near the disconnected cross-section. As usual for detachments in Mode I between FRP strips and masonry walls [51], the delamination occurred with the ripping of a thin layer of brick and mortar (Figure 51b). In fact, as far as the tensile strength is concerned, the substrate is the weakest element of the FRP/resin/masonry system, under Mode I.

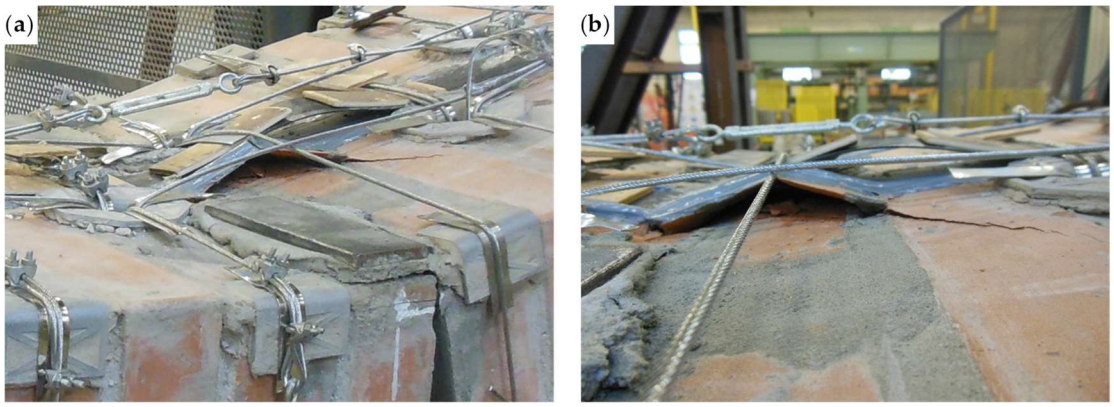

Figure 51.: Buckling of the upper CFRP strip: (**a**) how the transverse and longitudinal steel wire ropes hold back the upper CFRP strip, counteracting delamination on the middle cross-section and (**b**) detail of the brick peeling caused by delamination.

Even the delamination of the lower CFRP strip caused the detachment of a thin layer of substrate (Figure 48b), although the failure mode on the lower face of a bended specimen occurs in Mode II (Figure 40). Actually, the substrate is the weakest element also for shear sliding on mortar bed joints reinforced with FRP strips [52–54], since the substrate is the component with the lower shear strength in the FRP/resin/masonry system.

The significant decrease in load after the maximum load of Specimen W5 is a measure of the release of high energy that characterized delamination. However, as shown in Figure 49, the load of post-delamination began to rise to such an extent as to exceed the delamination load of Specimen W2. Actually, after the load recovering of post-delamination, the load/deflection diagram of Specimen W5 is almost superimposable to the load/deflection diagram of Specimen W4, at least up to the deflection value of about 47 *mm*. The superimposition between the two diagrams in the post-delamination phase indicates that the chosen type and amount of steel wire ropes are capable of bearing the same load of the steel ribbons of Specimen W4.

The load recovery after delamination is a consequence of the combined action of the transverse and longitudinal steel wire ropes on the CFRP strips. As far as the upper CFRP strip is concerned, Figure 51 shows how the combined action of the steel wire ropes led the upper CFRP strip to

delaminate only in part, allowing the non-delaminated portions of the strip to continue to contribute to the I-beam behavior established by the mechanical coupling. In particular, the longitudinal steel wire rope in the foreground of Figure 51a helps the underlying transverse steel wire rope to hold back the upper CFRP strip by providing a downward force at the intersection between the steel wire ropes, according to the simplified schemes of Figure 43a,b. The downward action of the longitudinal steel wire rope causes a change in the curvature of the transverse steel wire rope below (Figure 51a). However, due to the geometric effect of relative rotation caused by the inner hinge under the longitudinal steel wire rope, the downward action of the longitudinal steel wire rope would have been more significant if the holes for the passage of the longitudinal steel wire rope had been closer.

Despite the load recovering after delamination allowed Specimen W5 to exceed the delamination load of Specimen W2, it is worth remembering that a load drop of 15% to 20% is the limit usually considered satisfactory to avoid instability or damage problems in the adjacent structural elements of a real building, due to load redistribution. Therefore, the maximum load of Specimen W5 would probably represent the service limit of the second combined technique in a real application. Consequently, the main result obtained with the second combined technique does not lie in the load of post-delamination but in having increased the delamination load by approximately 139% with respect to the delamination load of Specimen W2. However, the existence of a long post-delamination branch together with the ability of the combined technique to establish a good box-type behavior even after damage has occurred (Section 1) allow us to affirm that also the second combined technique finds a second use beyond the structural limit, as a device for safeguarding life. Actually, both combined techniques can prevent the building from collapsing even if severely damaged, protecting people from possible injury.

For the load value of about 47 *mm*, the fraying became no longer sustainable by the remaining steel wire ropes and the longitudinal straps started to break in slow succession. The test ended without reaching the collapse of the specimen, when the operator recognized possible damage to the instrumentation for further increases in the vertical displacement of the loading piston. At the end of the test, only one of the longitudinal straps that crossed the disconnected cross-section was still resisting the load (the longitudinal strap passing through the restored hole in Figure 48b).

4. Conclusions

The combined technique discussed in this paper (the second combined technique) originates from the results of three-point bending flexural tests on a previous combined technique (the first combined technique), useful for improving the out-of-plane strength of masonry walls. The first combined technique exploits friction to mechanically couple CFRP strips and straps made of stainless steel ribbons. The effect of the mechanical coupling is an ideal I-beam behavior, capable of counteracting the out-of-plane displacements of masonry walls. The experimental result at the base of the second combined technique is that a greater stiffness of the straps seems to improve the performance of the ideal I-beam. Therefore, it seemed reasonable to replace the steel ribbons with the stiffer steel wire ropes, keeping the coupling technique between the straps and the CFRP strips unaltered.

After a preliminary phase that allowed the identification of the best performing fastening system for the steel wire ropes, a new three-point bending flexural test showed that the strap stiffness actually affects the behavior of the ideal I-beam. In particular, the second combined technique proved to be able to provide the reinforced specimen with greater stiffness for small deflections, when compared with the first combined technique. Actually, the stiffness of the specimen reinforced with the second combined technique is comparable to that of the specimen reinforced only with CFRP strips, while the first combined technique is more deformable.

Even more interesting are the results in terms of maximum load and ductility. In fact, the use of steel wire ropes delayed the delamination of the CFRP strips, increasing both the load and the deflection at the time of delamination. It is worth noting that even the steel ribbons increased both the load and the deflection at the time of delamination, but to a lesser extent. In particular, the second combined technique is much more effective than the first combined technique in increasing the

 doi:10.20944/preprints201907.0340.v1

delamination load. This, together with the increased delamination ductility, is a remarkable achievement for the second combined technique, since any traditional strengthening system acts on a structural element increasing either strength or ductility.

The increase in stiffness for small deflections, the greater maximum load, and the greater delamination deflection indicate that the ideal I-beam mechanism improves the behavior of the structural element even before delamination. On the contrary, with the first combined technique the ideal I-beam mechanism becomes evident only after delamination. Thus, the greater stiffness of the steel wire ropes makes it possible to make better use of the advantages of the mechanical coupling permitted by friction.

It is worth noting that the mechanical coupling modifies the resistant mechanisms of the coupled strengthening systems giving rise to a new resistant mechanism. In fact, the two combined techniques offer a strengthening effect similar to that of a buttress or other similar cross-bracing devices in the thickness of the wall. In contrast, both constituent strengthening systems are effective in the plane of the wall, if taken individually. Consequently, the strength parameters of the combined techniques are not the average values of the strength parameters of the two constituent strengthening systems.

As a last observation, the second combined technique also offers a post-delamination contribution similar to that of the first combined technique, with partial recovery of the load after delamination. In particular, the recovered post-delamination load exceeds the delamination load of the first combined technique. However, due to the high load drop caused by delamination, the importance of the load/deflection diagram after delamination does not lie in the recovered load but in the very existence of a post-delamination phase, which is a peculiarity of the combined techniques. In fact, this phase indicates that the I-beam mechanism survives delamination and—more importantly—the second combined technique is useful to avoid structural collapses up to high deflections. Therefore, as for the first combined technique, the second combined technique acts as a reinforcement system before the structural damage occurs and a life-protecting device after the structural damage has occurred. This makes the second combined technique very effective in offering protection against damage caused by the hammering actions provided by earthquakes [55], as well as by impact [56–60] and blast [61–65].

5. Future Developments

The analysis of the results on the second combined technique outlined some possible improvements to make the technique even more performing:

- In order to avoid that the breakage of one or more funnel-shaped elements interrupts the chain of the longitudinal straps, it may be useful to re-design the 3D-printed elements or use a more resistant material for the protective elements.
- In order to avoid that the geometric effects due to the relative rotations around the inner hinge make the action of the longitudinal straps vain on the transverse straps, it may be useful to decrease the length of the loops near the middle cross-section, where the inner hinge has the maximum probability of localization.
- In order to avoid that excessive post-delamination fraying leads to the collapse of the structural element, it may be useful to use longitudinal stainless steel ribbons in addition to the longitudinal steel wire ropes, at least near the middle cross-section. Since the function of the additional steel ribbons is only to safeguard life, they do not need a pre-tension.
- In order to avoid excessive load drops and dangerous release of energy at the time of delamination—which are mainly associated with the use of epoxy resins—it may be useful to replace the organic (epoxy resins) with an inorganic (mortar) matrix.

As for the last suggested improvement among those listed above, a possible solution consists in replacing the CFRP strips with textile-reinforced mortars (TRM) [66], also known in the international literature as textile reinforced concrete (TRC) [67] or fabric reinforced cementitious matrix (FRCM) [68] materials. In fact, TRMs combine high-strength fibers in the form of textiles (with open-mesh configuration) with inorganic matrices, such as cement or hydraulic-lime-based mortars.

The monotonic tensile tests on TRM specimens showed that the stress/strain curve of TRMs comprises three distinct linear branches [69]:

- First ascending branch: the specimen remains un-cracked.
- Horizontal branch (constant stress at increasing strains): multiple cracks develop in the mortar, after the first cracking. During this phase, the area of the resistant cross-section of the mortar decreases progressively [70–75], due to the gradual development of the crack pattern that causes a progressive transfer of the load from the matrix to the fibers of the textile.
- Second ascending branch, with a slope lower than that of the first branch: the crack pattern has fully developed and the increase in stress is due to the textile itself, until the fibers break.

The failure modes observed in bond tests performed on TRMs are [69]: (1) slippage of fibers through the mortar (the most common failure mode); (2) debonding of TRM with part of substrate; (3) debonding of TRM in the concrete–mortar interface; (4) debonding of TRM strips with part of substrate; and (5) rupture of TRM. Depending on which of these failure modes activates at the soffit of a bent beam, the loss of the strengthening action under bending load can be either progressive or abrupt [76]. It is precisely the possibility of designing a progressive failure of the TRM reinforcement system that deserves further study, to avoid excessive load drops and dangerous release of energy in the second combined technique, at the time of delamination.

As a final remark, a TRM strengthening technique can also allow us to avoid some of the typical drawbacks of FRPs when using the epoxy resin as interfacial adhesive as well as bonding matrix, namely, high costs, incompatibility with substrate materials, sensitivity to high temperatures and fire, and impossibility of application on wet surfaces. Actually, TRM is low-cost, compatible with concrete and masonry substrate materials, fire resistant, and usable on wet surfaces or at low temperatures.

Funding: This research received no external funding.

Acknowledgments: The results presented here are part of the CIMEST Scientific Research on the Identification of Materials and Structures, DICAM, Alma Mater Studiorum, Bologna (Italy). The author is grateful to Sofia Loreti for her active collaboration in the experimental program.

Conflicts of Interest: The author declares no conflict of interest.

References

1. Ferretti, E.; Pascale, G. Combined Strengthening Techniques to Improve the Out-of-Plane Performance of Masonry Walls. *Materials* **2019**, 1171.
2. Ferretti, E.; Pascale, G. Some of the Latest Active Strengthening Techniques for Masonry Buildings: A Critical Analysis. *Materials* **2019**, 1151.
3. Ferretti, E. Effectiveness of Active Confinement Techniques with Steel Ribbons: Masonry Buildings. *Eur. J. Eng. Form. Sci.* **2018**, *2*, 17–29.
4. Ferretti, E. Attaining a Beam-Like Behavior with FRP Strips and CAM Ribbons. *Eur. J. Eng. Formal Sci.* **2018**, *2*, 6–16.
5. Cilia, M.; Cipolla, I.; Colajanni, P.; Marnetto, R.; Recupero, A.; Spinella, N. Prove sperimentali su travi in c.a. rinforzate con metodo CAM®: Valutazione del comportamento a taglio. *Progettazione Sismica* **2015**, *VII*, 93–108.
6. Dolce, M.; Nigro, D.; Ponzo, F.C.; Marnetto, R. The CAM System for the Retrofit of Masonry Structures. In Proceedings of the 7th International Seminar on Seismic Isolation, Passive Energy Dissipation and Active Control of Vibrations of Structures, Assisi, Italy, 2–5 October 2001.
7. Dolce, M.; Ponzo, F.C.; Di Croce, M.; Moroni, C.; Giordano, F.; Nigro, D.; Marnetto, R. Experimental Assessment of the CAM and DIS-CAM Systems for the Seismic Upgrading of Monumental Masonry Buildings. In Proceedings of the PROHITECH 09, 1st International Conference on Protection of Historical Constructions, Rome, Italy, 21–24 June 2009; CRC Press/Balkema: Leiden, The Netherlands, 2009; pp. 1021–1028.

8. Dolce, M.; Ponzo, F.C.; Goretti, A.; Moroni, C.; Giordano, F.; De Canio, G.; Marnetto, R. 3D Dynamic Tests on 2/3 Scale Masonry Buildings Retrofitted with Different Systems. In Proceedings of the 14th World Conference on Earthquake Engineering, Beijing, China, 12–17 October 2008.
9. Leonori, M.; Vari, A. L'Influenza della Tipologia di Terreno sui Meccanismi Locali di Collasso degli Edifici in Muratura e Miglioramento Sismico con il Sistema CAM® [The Influence of the Type of Land on Local Mechanisms of Collapse of Masonry Buildings and Seismic Improvement with the CAM® System]. In *Dynamic Interaction of Soil and Structure (DISS_15), Proceedings of the 4th International Workshop on Archaeology, Cryptoportici, Hypogea, Geology, Geotechnics, Geophysics, Rome, Italy, 12–13 November 2015*; Monti, G., Valente, G., Eds.; DISS_Edition c/o DICEAA—L'Aquila University: L'Aquila, Italy, 2015; pp. 1–15.
10. Marnetto, R. Sviluppo ed applicazioni delle tecniche antisismiche presso la società TIS SpA di Roma. In Proceedings of the Seminario di Studi sui Sistemi e Tecnologie Antisismici, Rome, CNR, Italy, 12 September 2007; pp. 2–27.
11. Marnetto, R.; Vari, A. Linee Guida—Cuciture Attive per la Muratura: Procedura Generale per la Progettazione, Modellazione, Calcolo e Verifica di Edifici in Muratura Rinforzati con il Sistema di Cucitura Attiva CAM [Active Tying for Masonry: General Procedure for the Design, Modeling, Calculation, and Verification of Masonry Buildings Reinforced with the CAM Active Tying System]; EDIL CAM Sistemi S.r.l.: Rome, Italy, October 2015.
12. Marnetto, R.; Vari, A.; Marnetto, L.; Leonori, M. Conservare l'Edilizia in Muratura: Il Sistema CAM—Cuciture Attive dei Manufatti [Conserving the Building Heritage in Masonry: The CAM System—Active Confinement of Manufactured Buildings]; Edizioni PREprogetti: Rome, Italy, 2014.
13. Ministero delle Infrastrutture e dei Trasporti. Aggiornamento delle Norme Tecniche per le Costruzioni [Updating of the Technical Standards for Constructions]; Decreto; Gazzetta Ufficiale della Repubblica Italiana: Rome: Italy, 17 January 2018.
14. Presidente del Consiglio dei Ministri. Primi Elementi in materia di Criteri Generali per la Classificazione Sismica del Territorio Nazionale e Normative Tecniche per le Costruzioni in Zona Sismica [First Elements on the General Criteria for the Seismic Classification of the National Territory and Technical Regulations for Constructions in the Seismic Area]; Ordinanza n. 3274; Presidenza del Consiglio dei Ministri: Rome, Italy, 20 March 2003.
15. Bean Popehn, J.R.; Schultz, A.E.; Drake, C.R. Behavior of Slender, Posttensioned Masonry Walls under Transverse Loading. *J. Struct. Eng.-ASCE* **2007**, *133*, 1541–1550.
16. Bean Popehn, J.R.; Schultz, A.E.; Lu, M.; Stolarski, H.K.; Ojard, N.J. Influence of Transverse Loading on the Stability of Slender Unreinforced Masonry Walls. *Eng. Struct.* **2008**, *30*, 2830–2839.
17. Curtin, W.G.; Shaw, G.; Beck, J.K.; Howard, J. *Design of Post-Tensioned Brickwork*; The Brick Development Association: Windsor, UK, 1989.
18. Darbhanzi, A.; Marefat, M.S.; Khanmohammadi, M. Investigation of in-Plane Seismic Retrofit of Unreinforced Masonry Walls by means of Vertical Steel Ties. *Constr. Build. Mater.* **2014**, *52*, 122–129.
19. Dizhur, D.; Bailey, S.; Trowsdale, J.; Griffith, M.; Ingham, J.M. Performance of Posttensioned Seismic Retrofit of two Stone Masonry Buildings during the Canterbury Earthquakes. In Proceedings of the Australian Earthquake Engineering Society 2013 Conference, Hobart, Tasmania, Australia, 15–17 November 2013.
20. Ganz, H.R. Post-Tensioning Masonry Around the World. *Concr. Int.* **2003**, *25*, 65–69.
21. Ganz, H.R. Post-Tensioned Masonry Structures: Properties of Masonry, Design Considerations, Post-Tensioning System for Masonry Structures Applications; VSL Report Series No. 2; VSL International Ltd.: Berne, Switzerland, 1990.
22. Ismail, N.; Schultz, A.E.; Ingham, J.M. Out-of-Plane Seismic Performance of Unreinforced Masonry Walls Retrofitted using Post-Tensioning. In Proceedings of the 15th International Brick and Block Masonry Conference, Florianópolis, Santa Caterina, Brazil, 3–6 June 2012; Roman, H.R., Parsekian, G.A., Eds.; Federal University of Santa Catarina: Florianópolis, Brazil, 2012; pp. 1–12.
23. Ma, R.; Jiang, L.; He, M.; Fang, C.; Liang, F. Experimental Investigations on Masonry Structures using External Prestressing Techniques for Improving Seismic Performance. *Eng. Struct.* **2012**, *42*, 297–307.
24. Preciado, A. Seismic Vulnerability Reduction of Historical Masonry Towers by External Prestressing Devices. Ph.D. Thesis, Technical University of Braunschweig, Braunschweig, Germany; University of Florence, Florence, Italy, 2011.

25. Preciado, A.; Bartoli, G.; Budelmann, J.H. The use of Prestressing through Time as Seismic Retrofitting of Historical Masonry Constructions: Past, Present and Future Perspective. In *CIENCIA ergo-sum*; Universidad Autónoma del Estado de México: Toluca, México, 2015; Volume 22, pp. 242–252.
26. Schultz, A.E.; Scolforo, M.J. An Overview of Prestressed Masonry. *Mason. Soc. J.* **1991**, *10*, 6–21.
27. Sperbeck, S. Seismic Risk Assessment of Masonry Walls and Risk Reduction by means of Prestressing. Ph.D. Thesis, Technical University of Braunschweig, Braunschweig, Germany; University of Florence, Florence, Italy, 2009.
28. Spina, G.; Ramundo, F.; Mandara, A. Masonry Strengthening by Metal Tie-Bars, a Case Study. In Structural Analysis of Historical Constructions. In Proceedings of the Fourth International Seminar on Structural Analysis of Historical Constructions, Padova, Italy, 10–13 November 2004; Claudio, M., Paulo, B.L., Pere, R., Eds.; A.A. Balkema Publishers: Leiden, The Netherlands; London, UK; New York, NY, USA; Philadelphia, PA, USA; Singapore; Taylor & Francis Group: London, UK, 2005; pp. 1207–1213.
29. Van Eldere, H.; Ramos, L.F.; Verstrynge, E.; Shetty, N.; Van Balen, K.; Barroso, C.E.; Oliveira, D.V. The Application of Sonic Testing on Double-Leaf Historical Portuguese Masonry to Obtain Morphology and Mechanical Properties. *Rilem Bookseries* **2019**, *18*, 661–668.
30. Kariou, F.A.; Triantafyllou, S.P.; Bournas, D.A.; Koutas, L.N. Out-of-plane response of masonry walls strengthened using textile-mortar system. *Constr. Build. Mater.* **2018**, *165*, 769–781.
31. Koutas, L.N.; Bournas, D.A. Out-of-Plane Strengthening of Masonry-Infilled RC Frames with Textile-Reinforced Mortar Jackets. *J. Compos. Constr.* **2019**, *23*, 04018079.
32. Wang, C.; Sarhosis, V.; Nikitas, N. Strengthening/Retrofitting Techniques on Unreinforced Masonry Structure/Element Subjected to Seismic Loads: A Literature Review. *Open Construct. Build. Tech. J.* **2018**, *12*, 251–268.
33. Akhoundi, F.; Vasconcelos, G.; Lourenço, P.B. Experimental Out-Of-Plane Behavior of Brick Masonry Infilled Frames. *Int. J. Archit. Herit.* **2018**, doi:10.1080/15583058.2018.1529207.
34. Csikai, B.; Ramos, L.F.; Basto, P.; Moreira, S.; Lourenço, P.B. Flexural out-of-plane retrofitting technique for masonry walls in historical constructions. In Proceedings of the SAHC2014 9th International Conference on Structural Analysis of Historical Constructions, Mexico City, Mexico, 14–17 October 2014; Meli, R., Peña, F., Chávez, M., Eds.; 2014.
35. Lourenço, P.B. Technologies for Seismic Retrofitting and Strengthening of Earthen and Masonry Structures: Assessment and Application. In *Recent Advances in Earthquake Engineering in Europe, ECEE 2018, Geotechnical, Geological and Earthquake Engineering*, Pitilakis, K., ed.; Springer: Cham, Switzerland, 2018; Volume 46, pp. 501–518.
36. Corradi, M.; Di Schino, A.; Borri, A.; Rufini, R. A Review of the use of Stainless Steel for Masonry Repair and Reinforcement. *Constr. Build. Mater.* **2018**, *181*, 335–346.
37. Borri, A.; Corradi, M.; Castori, G.; Molinari, A. Stainless steel strip - A proposed shear reinforcement for masonry wall panels. *Constr. Build. Mater.* **2019**, *211*, 594–604.
38. Ferretti, E. Shape-Effect in the Effective Laws of Plain and Rubberized Concrete. *CMC-Comput. Mater. Con.* **2012**, *30*, 237–284.
39. Ferretti, E. On nonlocality and Locality: Differential and Discrete Formulations. In Proceedings of the ICF11, 11th International Conference on Fracture 2005, Turin, Italy, 20–25 March 2005; Carpinteri, A., Ed.; Eigenverl: 2005; Curran Associates, Inc.: Red Hook, NY, USA, 2010; pp. 1728–1733.
40. Ferretti, A local strictly nondecreasing material law for modeling softening and size-effect: a discrete approach. *CMES-Comp. Model. Eng.* **2005**, *9*, 19–48.
41. Rousakis, T.C.; Panagiotakis, G.D.; Archontaki, E.E.; Kostopoulos, A.K. Prismatic RC columns externally confined with FRP sheets and pretensioned basalt fiber ropes under cyclic axial load. *Compos. B Eng.* **2019**, *163*, 96–106.
42. Llorens, J. Fabric Structures in Architecture; Editor: Llorens, J., Imprint: Woodhead Publishing, 2015.
43. Ferretti, E. A Cell Method Stress Analysis in Thin Floor Tiles Subjected to Temperature Variation. *CMC-Comput. Mater. Con.* **2013**, *36*, 293–322.
44. Ferretti, E. Cell method analysis of crack propagation in tensioned concrete plates. *CMES-Comp. Model. Eng.* **2009**, *54*, 253–281.
45. Ferretti, E. Modeling of the pullout test through The Cell Method. In Proceedings of the International Conference on Restoration, Recycling and Rejuvenation Technology for Engineering and Architecture

Application, RRRTEA '04, Cesena, Italy; Sih, G.C., Nobile, L., Eds.; Aracne: Cesena, Italy, 2004; pp. 180–192.

46. Ferretti, E. Satisfying Boundary Conditions in Homogeneous, Linear-Elastic and Isotropic Half-Spaces Subjected to Loads Perpendicular to the Surface: Distributed Loads on Adjacent Contact Areas. *Curved and Layer. Struct*. **2019**, *6*, 11–29.
47. Ferretti, E. The Second Order Solution of Boussinesq's Problem. In Research and Applications in Structural Engineering, Mechanics and Computation - Proceedings of the 5th International Conference on Structural Engineering, Mechanics and Computation, SEMC 2013, Cape Town, South Africa; 2013, pp. 2473–2478.
48. Ferretti, E. Waste Tire Rubberized Concrete Plates for Airport Pavements: Stress and Strain Profiles in Time and Space Domains. *CMC-Comput. Mater. Con*. **2012**, *31*, 87–111.
49. Ferretti, E. A Higher Order Solution of the Elastic Problem for a Homogeneous, Linear-Elastic and Isotropic Half-Space Subjected to a Point-Load Perpendicular to the Surface. *CMES-Comp. Model. Eng*. **2012**, *86*, 435–468.
50. Ferretti, E.; Bignozzi, M.C. Stress and Strain Profiles along the Cross-Section of Waste Tire Rubberized Concrete Plates for Airport Pavements. *CMC-Comput. Mater. Con*. **2012**, *27*, 231–273.
51. Oliveira, D.V.; Basilio, I.; Lourenco, P.B. Experimental Bond Behavior of FRP Sheets Glued on Brick Masonry. *J. Compos. Constr*. **2010**. *15*, 32–41, DOI:10.1061/(ASCE)CC.1943-5614.0000147.
52. de Felice, G.; Aiello, M.A.; Bellini, A.; Ceroni, F.; De Santis, S.; Garbin, E.; Leone, M.; Lignola, G.P.; Malena, M.; Mazzotti, C.; Panizza, M.; Valluzzi, M.R. Experimental characterization of composite-to-brick masonry shear bond. *Mater. Struct*. **2015**, 2581–2596.
53. Panizza M.; Garbin, E.; Valluzzi, M.R.; Modena, C. Experimental study of the bond of FRP applied to natural stones and masonry prisms. *Key Eng. Mater.* **2014**, *624*, 453–460.
54. Panizza M.; Garbin, E.; Valluzzi, M.R. Peel strength testing of FRP applied to clay bricks. In Proceedings of FraMCoS-8, VIII International Conference on Fracture Mechanics of Concrete and Concrete Structures, Toledo, Spain, 10–14 March 2013; Van Mier, J.G.M., Ruiz, G., Andrade, C., Yu, R.C., and Zhang, X.X. Eds., 2013; 9 pp.
55. Belghiat, C.; Messabhia, A.; Plassiard, J.-P.; Guenfoud, M.; Plé, O.; Perrotin, P. Experimental Study of Double-Panel Confined Masonry Walls under Lateral Loading. *J. Build. Eng*. **2018**, *20*, 531–543.
56. Sauer, C.; Heine, A.; Riedel, W. Comprehensive Study of Projectile Impact on Lightweight Adobe Masonry. *Int. J. Impact Eng*. **2019**, *125*, 56–62.
57. Bonacho, J.; Oliveira, C.S. Multi-Hazard Analysis of Earthquake Shaking and Tsunami Impact. *IJDRS Int. J. Disaster Risk Reduct.* **2018**, *31*, 275–280.
58. Lonetti, P.; Maletta, R. Dynamic Impact Analysis of Masonry Buildings Subjected to Flood Actions. *Eng. Struct*. **2018**, *167*, 445–458.
59. Pourfalah, S.; Cotsovos, D.M.; Suryanto, B.; Moatamedi, M. Out-of-Plane Behaviour of Masonry Specimens Strengthened with ECC under Impact Loading. *Eng. Struct*. **2018**, *173*, 1002–1018.
60. Pham, T.M.; Hao, H. Impact Behavior of FRP-Strengthened RC Beams without Stirrups. *J. Compos. Constr*. **2016**, *20*, 4016011.
61. Goswami, A.; Adhikary, S.D. Retrofitting Materials for Enhanced Blast Performance of Structures: Recent advancement and challenges ahead. *Constr. Build. Mater*. **2019**, *204*, 224–243.
62. Li, Z.; Zhang, X.; Shi, Y.; Xu, Q. Experimental Studies on Mitigating Local Damage and Fragments of Unreinforced Masonry Wall under Close-in Explosions. *J. Perform. Constr. Facil*. **2019**, *33*, 04019009.
63. Michaloudis, G.; Gebbeken, N. Modeling Masonry Walls under Far-Field and Contact Detonations. *Int. J. Impact Eng*. **2019**, *123*, 84–97.
64. Russo, P.; De Marco, A.; Parisi, F. Failure of Reinforced Concrete and Tuff Stone Masonry Buildings as Consequence of Hydrogen Pipeline Explosions. *Int. J. Hydrog. Energy* **2019**, in press.
65. Alsayed, S.H.; Elsanadedy, H.M.; Al-Zaheri, Z.M.; Al-Salloum, Y.A.; Abbas, H. Blast Response of GFRP-Strengthened Infill Masonry Walls. *Constr. Build. Mater*. **2016**, *115*, 438–451.
66. Triantafillou, T.C.; Papanicolaou, C.G. Shear strengthening of reinforced concrete members with textile reinforced mortar (TRM) jackets. *Mater. Struct*. **2006**, *39*, 93–103.
67. Ortlepp, R.; Hampel, U.; Curbach, M. A new approach for evaluating bond capacity of TRC strengthening. *Cem. Concr. Compos*. **2006**, *28*, 589–597.
68. D'Ambrisi, A.; Feo, L.; Focacci, F. Bond-slip relations for PBO-FRCM materials externally bonded to concrete. *Compos. Part B: Eng*. **2012**, *43*, 2938–2949.

69. Koutas, L.N.; Tetta, Z.; Bournas, D.A.; Triantafillou, T.C. Strengthening of Concrete Structures with Textile Reinforced Mortars: State-of-the-Art Review. *J. Compos. Constr.* **2019**, *23*, 03118001.
70. Ferretti, E.; Di Leo, A. Cracking and creep role in displacements at constant load: Concrete solids in compression. *CMC-Comput. Mater. Con.* **2008**, *7*, 59–79.
71. Ferretti, E. A Discrete Nonlocal Formulation using Local Constitutive Laws. *Int. J. Fract.* **2004**, *130*, L175–L182.
72. Ferretti, E. On Strain-softening in dynamics. *Int. J. Fract.* **2004**, *126*, L75–L82.
73. Ferretti, E. Experimental procedure for verifying strain-softening in concrete. *Int. J. Fract.* **2004**, *126*, L27–L34.
74. Ferretti, E. A discussion of strain-softening in concrete. *Int. J. Fract.* **2004**, *126*, L3–L10.
75. Ferretti, E.; Di Leo, A.; Viola, E. A Novel Approach for the Identification of Material Elastic Constants. In *Problems in Structural Identification and Diagnostics: General Aspects and Application. International Centre for Mechanical Sciences (Book Series: CISM Courses and Lectures)*. Davini, C., Viola, E., Eds.; Springer-Verlag Wien: Vienna, Austria, 2003; Volume 471, pp. 117–131.
76. D'Ambrisi, A.; Focacci, F. Flexural strengthening of RC beams with cement-based composites. *J. Compos. Constr.* **2011**, *15*, 707–720.